

## PREGNANCY

## PBX1 expression in uterine natural killer cells drives fetal growth

Yonggang Zhou<sup>1,2,3</sup>, Binqing Fu<sup>1,2\*</sup>, Xiuxiu Xu<sup>1,2</sup>, Jinghe Zhang<sup>1,2</sup>, Xianhong Tong<sup>3</sup>, Yanshi Wang<sup>3</sup>, Zhongjun Dong<sup>4</sup>, Xiaoren Zhang<sup>5</sup>, Nan Shen<sup>6</sup>, Yiwen Zhai<sup>7</sup>, Xiangdong Kong<sup>7</sup>, Rui Sun<sup>1,2</sup>, Zhigang Tian<sup>1,2\*</sup>, Haiming Wei<sup>1,2\*</sup>

Copyright © 2020  
The Authors, some  
rights reserved;  
exclusive licensee  
American Association  
for the Advancement  
of Science. No claim  
to original U.S.  
Government Works

Abundant decidual natural killer (dNK) cells at the maternal-fetal interface are important during early pregnancy. However, functional subsets of dNK cells remain poorly understood. We describe a CD49a<sup>+</sup>PBX homeobox 1 (PBX1)<sup>+</sup> dNK cell subset that promotes fetal development in humans and mice. The expression of PBX1 in dNK cells is up-regulated via the activated AKT1 pathway through the interaction of major histocompatibility complex G with the immunoglobulin-like transcript 2 receptor. PBX1 drives pleiotrophin and osteoglycin transcription in dNK cells, further promoting fetal development. Decreased PBX1 expression or the PBX1<sup>G215</sup> mutant correlated with fetal growth restriction and pregnancy failure in patients with unexplained recurrent spontaneous abortion (URSA). Inactivation of *Pbx1* in mouse dNK cells impairs fetal development by decreasing growth-promoting factors from CD49a<sup>+</sup>PBX1<sup>+</sup> dNK cells. Impairment of PBX1 in dNK cells has positive correlation with URSA pathogenesis and may provide a potential marker for this condition.

## INTRODUCTION

Advances in the study of natural killer (NK) cells in their microenvironments are changing our understanding of immune system contributions to the maintenance of tissue homeostasis (1–3). During the first trimester of pregnancy, decidual NK (dNK) cells are the dominant lymphocyte in human decidua, comprising up to 70% of leukocytes (4). Single-cell sequencing data show that heterologous receptor expression on dNK cells can generate diverse receptor-ligand combinations, suggesting that dNK cells have multiple functional subsets related to immune tolerance, embryo development, and pregnancy success (4–6). Although the reduction and dysfunction of NK cells at the maternal-fetal interface contribute to pregnancy-related diseases (4, 7, 8), including unexplained recurrent spontaneous abortion (URSA) (9–11), a complex disorder affecting about 1 to 5% of women of childbearing age (12–14), the transcriptional regulatory mechanisms determining dNK functional subsets under physiological and pathological conditions have not been defined.

dNK cell numbers increase rapidly during early pregnancy, accompanied by secretion of a complex array of factors with multiple functions and exhibiting low cytotoxicity relative to peripheral NK (pNK) cells (8, 15). During natural allogenic pregnancies, CD27<sup>+</sup> dNK cells produce interferon- $\gamma$  (IFN- $\gamma$ ) to inhibit inflammatory T helper 17 (T<sub>H</sub>17) cell responses and maintain immune tolerance at the maternal-fetal interface (9). IFN- $\gamma$  secreted by dNK cells can

also activate angiogenesis-related gene expression and promote spiral artery remodeling (16). Furthermore, dNK cells can directly promote vascular growth in the decidual tissue by producing vascular endothelial growth factor (VEGF) and placental growth factor (17). In repeat pregnancies, dNK cells exhibit a “pregnancy-trained” phenotype, with increased IFN- $\gamma$  and VEGF production, and up-regulation of immunoglobulin-like transcript 2 (ILT2) (18). In addition, dNK cells also have the potential to acquire cytotoxic activity in the decidual microenvironment in the presence of infection (19).

The number of dNK cells increases rapidly during placenta formation in the first trimester and subsequently decreases quickly (20, 21), suggesting that dNK cells may also help to nourish the early fetus. In a previous report, we demonstrated that CD49a<sup>+</sup> dNK cells can respond to extravillous trophoblast (EVT)-derived major histocompatibility complex G [human leukocyte antigen G (HLA-G)] signaling through ILT2, stimulating production of growth-promoting factors (GPFs) including pleiotrophin (PTN) and osteoglycin (OGN), which promote early fetal development (11). This study provides insight into the function of NK cell subsets in the uterine microenvironment during pregnancy (8, 22, 23). The identification of such functional subsets indicates that their activities may be regulated by specific transcription factors. PBX homeobox 1 (PBX1) is a transcription factor belonging to the TALE (three-amino acid loop extension) family of homeodomain proteins that acts during B cell development (24–26). Here, we evaluated PBX1 expression in CD49a<sup>+</sup> dNK cells and investigated whether PBX1 can directly regulate the transcriptional expression of GPFs in dNK cells. Moreover, we evaluated the effects of PBX1 loss in dNK cells on URSA etiology compared with physiological status.

## RESULTS

## PBX1 is expressed in dNK cells producing GPFs

We performed comparative transcriptome-wide screening to assess dNK and pNK cell transcription factor expression profiles. The transcription factor *PBX1* was identified as preferentially expressed in dNK cells by RNA sequencing (RNA-seq) (Fig. 1A). This finding

<sup>1</sup>Division of Molecular Medicine, Hefei National Laboratory for Physical Sciences at Microscale, The CAS Key Laboratory of Innate Immunity and Chronic Disease, School of Life Sciences, University of Science and Technology of China, Hefei, Anhui 230027, China. <sup>2</sup>Institute of Immunology, University of Science and Technology of China, Hefei, Anhui 230027, China. <sup>3</sup>First Affiliated Hospital, University of Science and Technology of China, Hefei, Anhui 230026, China. <sup>4</sup>School of Medicine, Tsinghua University, Beijing 100086, China. <sup>5</sup>CAS Key Laboratory of Tissue Microenvironment and Tumor, Shanghai Institute of Nutrition and Health, University of Chinese Academy of Sciences, Chinese Academy of Sciences, Shanghai 200025, China. <sup>6</sup>Shanghai Institute of Rheumatology, Renji Hospital, School of Medicine, Shanghai Jiao Tong University, Shanghai 200001, China. <sup>7</sup>Center for Genetic and Prenatal Diagnosis, Department of Gynecology and Obstetrics, the First Affiliated Hospital of Zhengzhou University, Zhengzhou, Henan 450052, China.

\*Corresponding author. Email: ustcwhm@ustc.edu.cn (H.W.); tgz@ustc.edu.cn (Z.T.); fbq@ustc.edu.cn (B.F.)

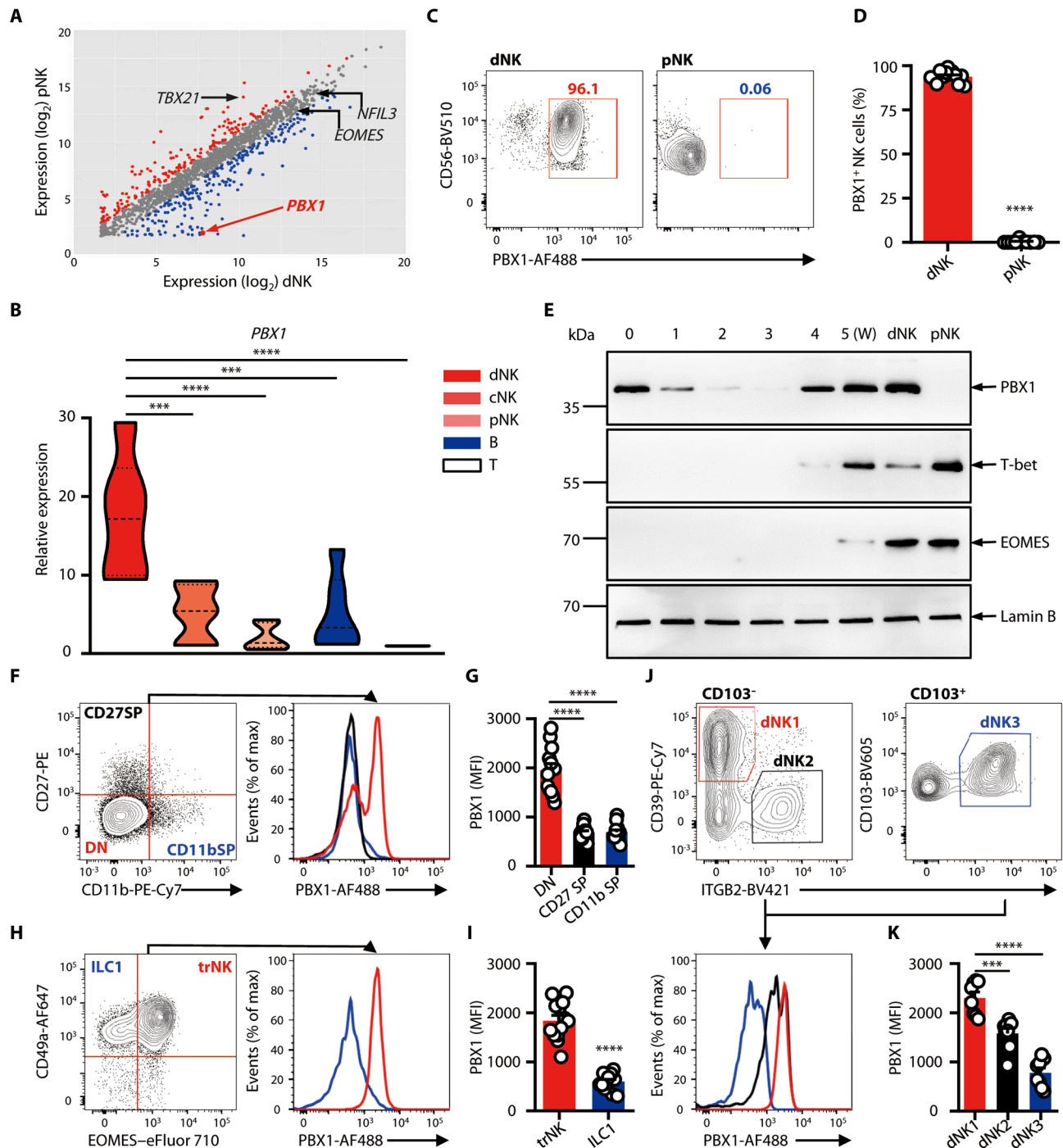


**Fig. 1. Identification of PBX1 in NK cells at the maternal-fetal interface.** (A) RNA-seq transcription factor data from human dNK and pNK cells [GSE97217; (11)]. (B) The qPCR analysis of *PBX1* in purified dNK ( $n = 6$ ) and cord blood NK (cNK) cells ( $n = 6$ ) and NK (pNK), B, and T cells from peripheral blood ( $n = 6$ ), normalized to its expression in T cells (\*\* $P < 0.001$  and \*\*\*\* $P < 0.0001$  by ANOVA). (C and D) Representative flow cytometry data for *PBX1* (C) and percentages of *PBX1*<sup>+</sup> NK cell subsets (D) in gated  $CD3^+CD45^+CD56^+$  dNK ( $n = 13$ ) and pNK cells ( $n = 10$ ) (\*\*\*\* $P < 0.0001$  by two-tailed  $t$  test). Numbers in (C) are percentages of NK cell subsets. (E) Western blot analysis of *PBX1*, T-bet, EOMES, and Lamin B in dNK cells, pNK cells, and cells harvested from the decidual-like NK cell in vitro culture system at 0, 1, 2, 3, 4, and 5 weeks. W, week. Lamin B is used as an internal control. (F to I) NK cells were isolated from healthy decidua of first-trimester pregnancies ( $n = 13$ ) and gated for  $CD3^+CD45^+CD56^+$  cells. (F and G) Representative flow cytometry evaluating *PBX1* expression (F) and statistical analysis of mean fluorescence intensity (MFI) (G) in the dNK cell subset (gated on CD11b and CD27 expression) (\*\*\*\* $P < 0.0001$  by ANOVA). DN (red), CD11b<sup>-</sup>CD27<sup>-</sup>; CD27 SP (black), CD11b<sup>-</sup>CD27<sup>+</sup>; CD11b SP (blue), CD11b<sup>+</sup>CD27<sup>-</sup>. (H and I) Representative flow cytometry evaluating *PBX1* expression (H) and statistical analysis of MFI (I) in trNK (red) cells (\*\*\*\* $P < 0.0001$  by two-tailed  $t$  test), gated on CD49a<sup>+</sup>EOMES<sup>-</sup> ILC1 (blue) and CD49a<sup>+</sup>EOMES<sup>+</sup>. (J and K) Representative flow cytometry of *PBX1* expression (J) and statistical analysis of MFI (K) in gated CD39<sup>+</sup>CD49a<sup>+</sup>CD103<sup>-</sup>ITGB2<sup>-</sup> dNK1 (red), CD39<sup>-</sup>CD49a<sup>+</sup>CD103<sup>-</sup>ITGB2<sup>+</sup> dNK2 (black), and CD49a<sup>+</sup>CD103<sup>+</sup>ITGB2<sup>+</sup> dNK3 (blue) cells ( $n = 8$ ) (\*\*\* $P < 0.001$  and \*\*\*\* $P < 0.0001$  by ANOVA).

was validated by quantitative polymerase chain reaction (qPCR), which demonstrated that dNK cells predominantly express *PBX1* relative to NK cells from different tissues, B cells, and T cells (Fig. 1B). Flow cytometric analyses using the anti-PBX1 rat monoclonal antibody (fig. S1) showed that dNK, but not pNK, cells produce PBX1 (Fig. 1, C and D, and fig. S2A). PBX1 staining of purified dNK and pNK cells confirmed this result by immunofluorescence (fig. S2B).

We next analyzed amino acid homology among NK cell-associated transcription factors and found that PBX1 was highly conserved: In model mammals, the amino acid sequence was completely identical to that of humans (fig. S2C). Furthermore, PBX1 is widely expressed across species (fig. S2D) and functions in the formation of lymphocyte precursors (24, 25). To distinguish between the effects of PBX1 on NK cell precursor development and mature cell function, we established an in vitro system for induction of dNK-like cell development by stimulation of human CD34<sup>+</sup> cord blood hematopoietic stem cells with a cytokine cocktail (fig. S3A). After 5 weeks, dNK-like cells were obtained (purity, >90%) (fig. S3B), and results by qPCR showed that *PBX1* increased during the past 2 weeks of cell culture (fig. S3C). Protein assays confirmed that PBX1 was expressed in precursor cells and that PBX1 protein was higher in mature dNK cells (Fig. 1E), suggesting that PBX1 may regulate the function of mature dNK cells.

NK cell functions can be orchestrated through cross-talk with invasive decidual stromal cells or trophoblasts via receptor-ligand interactions (4, 5, 11, 17, 27), which implies that heterogeneous dNK cells may contain diverse functional subsets. A subset of dNK cells expressing CD11b and CD27, or CD49a and eomesodermin (EOMES), are activated by trophoblast HLA-G signaling to produce GPFs that induce fetal development (11, 22, 23). PBX1 was highly expressed in CD11b<sup>+</sup>CD27<sup>+</sup> dNK cells and CD49a<sup>+</sup>EOMES<sup>+</sup> tissue-resident NK (trNK) cells (Fig. 1, F to I). Single-cell sequencing of samples from the maternal-fetal interface confirmed the presence of the dNK1 (CD39<sup>+</sup>CD49a<sup>+</sup>CD103<sup>+</sup>ITGB2<sup>-</sup>) cell subset, with high HLA-G receptor expression, and PBX1 was also highly expressed in this subset (Fig. 1, J and K). Therefore, we hypothesized that HLA-G signaling may drive *PBX1* expression in dNK cells, thereby promoting GPFs production.

### The HLA-G-ILT2-AKT axis drives PBX1 expression

We used CSP100 Plus signaling pathway antibody microarrays to analyze changes in signaling pathways in dNK cells cocultured with and without EVT cells. This approach enabled simultaneous quantitative analysis of 16 signaling pathways common and important in biomedical research. Phosphatidylinositol 3-kinase (PI3K)-Akt signaling pathway-related proteins and phosphorylation were altered in dNK cells cocultured with EVT cells (Fig. 2A). Specifically, AKT1 phosphorylation at position 473 was increased, while phosphorylation at residue 308, and its regulatory kinase PDK1, was not obviously altered (Fig. 2, B and C). Furthermore, we verified increased PDK2, phosphorylation of AKT1 at position 473, and PBX1 in dNK cells cocultured with EVT cells by protein analysis (Fig. 2D). We found that PBX1 expression was reduced by small interfering RNA (siRNA) targeting *PDK2* and *AKT1* and by treatment with AKT1 phosphorylation inhibitor (AKTi-1/2) to impair AKT1 activation in dNK cells cocultured with EVT cells (Fig. 2, E to G). These results suggested that, in coculture with EVT cells, dNK cells up-regulate PBX1 expression via PDK2-promoted pAKT1<sup>473</sup>.

To further investigate whether EVT-derived HLA-G and ILT2 interactions can promote phosphorylation of AKT1 at position 473 in dNK cells, we added blocking antibodies that antagonize HLA-G and ILT2 into the coculture system. Blocking of HLA-G or ILT2 inhibited AKT1 phosphorylation and impaired PBX1 expression in dNK cells (Fig. 2H). These results indicate that EVT-derived HLA-G promotes AKT1 activation in dNK cells by interacting with ILT2, thereby driving expression of PBX1 (Fig. 2I).

### PBX1 promotes transcription of GPFs

PTN and OGN are the two major GPFs secreted by dNK cells (11). To investigate whether PBX1 regulates *PTN* and *OGN* mRNA expression in dNK cells, we used the online database TFBIND (<http://tfbind.hgc.jp/>) to analyze potential binding sites in the promoters of these genes. The *PTN* and *OGN* promoters contained multiple potential PBX1-binding sites (Fig. 3A), suggesting that PBX1 may regulate their expression. Overexpression of *PBX1* in the dNK-like cell induction system using a lentiviral vector (fig. S3, A, D, and E) led to significantly higher PTN ( $P = 0.0012$ ) and OGN ( $P = 0.005$ ) expression than in mock-infected cells (fig. S3, F and G), confirming the positive regulation of PTN and OGN by PBX1. T-box transcription factor 21 (T-bet), EOMES, and phosphorylated S6 ribosomal protein [pS6; a marker of mTOR (mammalian target of rapamycin) activity] expression were also increased on *PBX1* overexpression (fig. S3, H and I). Next, purified human dNK cells were transfected with siRNA targeting *PBX1* (fig. S3J) and cocultured with EVT cells to provide activation signals. PTN and OGN mRNA ( $P < 0.0001$ ; fig. S3K) and protein ( $P < 0.0001$ ; Fig. 3, B and C) expression were significantly decreased in the *PBX1* knockdown group. These data demonstrate that PBX1 promotes *PTN* and *OGN* expression in dNK cells.

To determine whether PBX1 directly binds to the *PTN* and *OGN* promoters in purified human dNK cells, we conducted chromatin immunoprecipitation (ChIP) with anti-PBX1 antibody, followed by high-throughput DNA sequencing (ChIP-seq). Individual PBX1-binding peaks were identified in the *PTN* and *OGN* promoters, indicating that PBX1 can bind directly to these sites (Fig. 3D and fig. S3, L and M). Sequence analysis of eluted DNA fragments revealed that the PBX1-binding motif in the *PTN* promoter was 5'-ATCATTTAAA-3' [at -486 to -478 base pairs (bp)], with 5'-TTGATTGTG-3' (at -1979 to -1971 bp) and 5'-ATCATTTAAA-3' (at -213 to -205 bp) in the *OGN* promoter (Fig. 3E). The two identified PBX1-binding motifs were highly consistent with sequences previously reported in tumor cells and macrophages (28). Immunoprecipitation of PBX1 from dNK cells confirmed that the PBX1 antibodies used for ChIP-seq were specific (Fig. 3F). Analysis of dNK cell ChIP products from humans and mice expressing a PBX1 fusion protein with the hemagglutinin (HA) tag inserted at the N terminus by qPCR validated the ChIP-seq data (Fig. 3, G and H). Furthermore, Western blotting showed that PBX1 can bind these specific sequences in nuclear lysates from 293T cells overexpressing PBX1 (Fig. 3I). For functional analysis of these binding sites, we constructed luciferase reporter plasmids containing the *PTN* (-603 to -53 bp) and *OGN* (-2100 to -1500 bp and -654 to -100 bp) promoter PBX1-binding motifs, respectively (Fig. 3J). Luciferase expression activity demonstrated that the inserted PBX1-binding domains were active in 293T cells (Fig. 3K), with PBX1 up-regulating expression of *PTN* and *OGN* by directly binding to these promoter-specific motifs from human and mouse dNK cells.

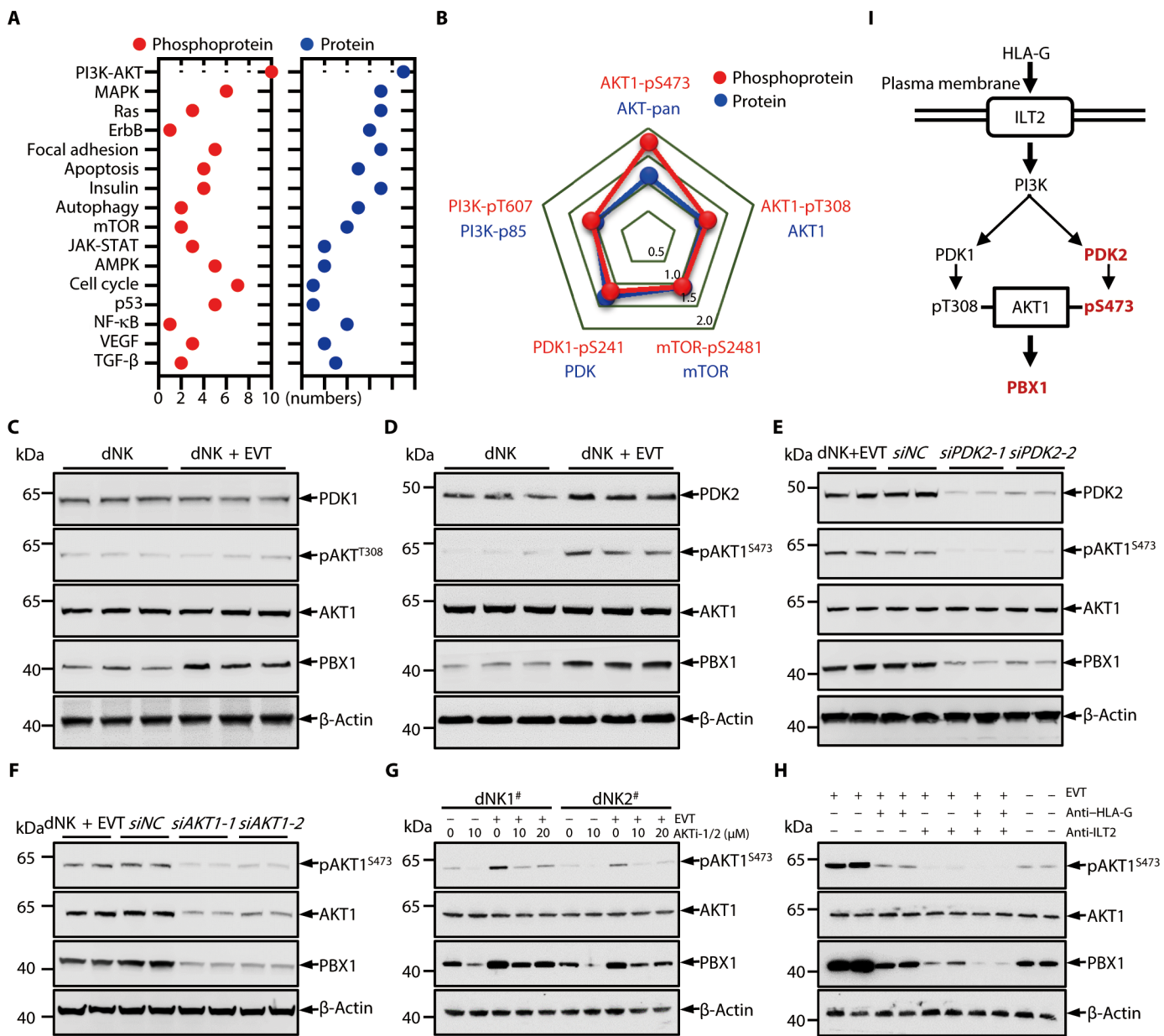


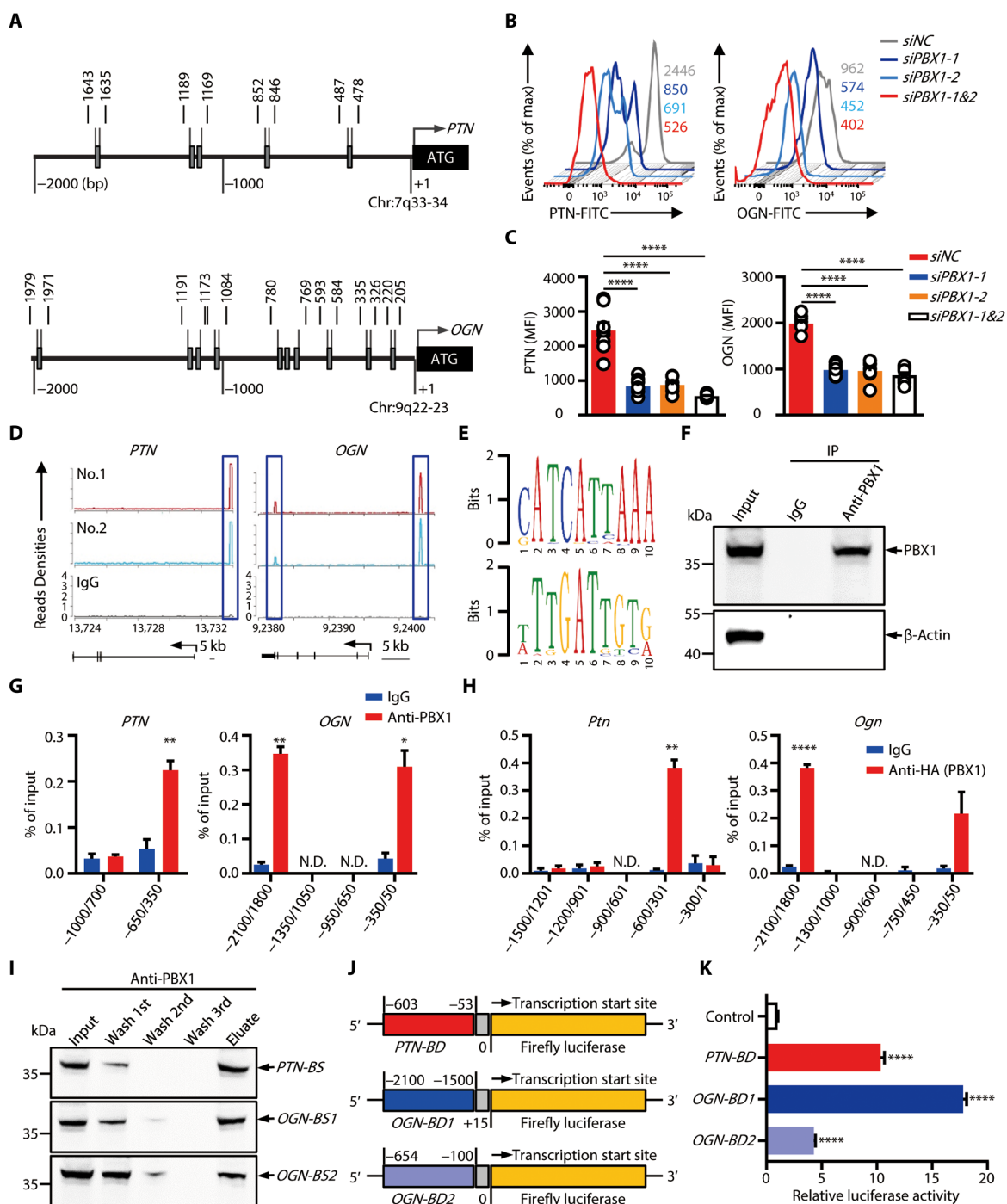
**Fig. 2. HLA-G promotes PBX1 expression in NK cells by activating AKT.** (A and B) Enriched pathways in human dNK cells and dNK cells in coculture with EVT cells based on an antibody microarray for profiling protein content and phosphorylation. Untreated dNK cells served as controls. (A) Scatter plot of the number of proteins (blue)/phosphorylated sites (red) whose signal value is up or down more than 1.5-fold in the corresponding pathway in dNK cells cocultured with EVT cells. Numbers indicate the amount of protein. (B) Radar chart of signal value of the key kinases in the AKT signaling pathway demonstrating enrichment of differentially expressed (blue) and phosphorylated proteins (red) in dNK cells cocultured with EVT cells. Numbers are fold change in signal value of proteins/phosphorylated sites. PI3K, phosphatidylinositol 3-kinase; MAPK, mitogen-activated protein kinase; mTOR, mammalian target of rapamycin; JAK-STAT, Janus kinase–signal transducer and activator of transcription; VEGF, vascular endothelial growth factor; TGF-β, transforming growth factor-β. (C and D) Western blot analysis of PDK1, pAKT<sup>308</sup> (C), PDK2, pAKT<sup>5473</sup> (D), AKT1, and PBX1 in dNK cells and dNK cells cocultured with EVT cells. (E) Western blot analysis of PDK2, pAKT<sup>473</sup>, AKT1, and PBX1 in purified human dNK cells transfected with *siRNA-PDK2* and cocultured with EVT cells. (F and G) Western blot analysis of pAKT<sup>473</sup>, AKT1, and PBX1 in purified human dNK cells transfected with *siRNA-AKT1* (F) or treated with AKTi-1/2 (G) and cocultured with EVT cells. NC, negative control. Experiments (C to G) were independently performed three times. (H) Western blot analysis of pAKT<sup>473</sup>, AKT1, and PBX1 in purified human dNK cells cocultured with EVT cells with or without anti-HLA-G or anti-ILT2 antibody. Experiment was independently performed twice with similar results. β-Actin in (C) to (H) is used as an internal reference. (I) Working diagram of AKT1 activation driving PBX1 expression.

**Impaired PBX1 activity in dNK cells from patients with URSA**  
 CD49a is a marker of typical trNK cells (29, 30), including those from human and mouse decidual tissue (4, 11, 31). We gated dNK cells from 12 patients with URSA by flow cytometry to analyze

PBX1 protein expression. Gating of dNK cells on CD49a and PBX1 demonstrated that the proportion and number of CD49a<sup>+</sup>PBX1<sup>+</sup> dNK cells were significantly reduced in patients with URSA ( $P < 0.0001$ ; Fig. 4, A and B). Analysis of the expression of PBX1 in GFP-producing

**Fig. 3. PBX1 enhances the transcription of *PTN* and *OGN* in NK cells.**

**(A)** Schematic structure of the human *PTN* (above) and *OGN* (below) promoters with potential PBX1-binding sites. **(B and C)** Representative intracellular flow cytometry (B) and statistical analysis of the MFI (C) of *PTN* and *OGN* in purified human dNK cells ( $n=8$ ) transfected with siRNA-*PBX1* or siRNA-NC (negative control) and cocultured with EVT cells (\*\*\*\* $P < 0.0001$  by ANOVA). The numbers in (B) indicate the MFI for each GFP. **(D)** ChIP-seq tracks show binding peaks for PBX1 at the *PTN* and *OGN* loci in human dNK cells. No.1 and no.2 indicate data of two experimental replicates generated using the anti-PBX1 antibody, IgG antibody, negative control. Binding regions are marked by rectangular boxes. **(E)** The PBX1 DNA binding motif was determined by sequence analysis of binding regions. **(F)** Western blot analysis of PBX1 immunoprecipitates (IP) from human dNK cells.  $\beta$ -Actin is used as an internal control. **(G and H)** Quantitative RT-PCR of the DNA precipitated by ChIP with anti-PBX1 antibody for PBX1 binding to the *PTN* and *OGN* promoters in human dNK cells (G) and IL-15-expanded NK cells from *Pbx1*<sup>HA-tag</sup> knock-in mice (H) (\*\* $P < 0.05$ , \*\* $P < 0.01$ , and \*\*\*\* $P < 0.0001$  by two-tailed  $t$  test). N.D., no data. **(I)** Western blot analysis to detect PBX1 in DNA pull-down assays using *PTN*- or *OGN*-binding site probes in 293T cells. BS, binding site. **(J)** Schematic representation of pGL3-based luciferase reporter constructs containing the putative PBX1-binding domains from the *PTN* and *OGN* promoters. BD, binding domain. **(K)** Relative luciferase activities in 293T cells transfected with *PTN*-BD or *OGN*-BD reporter vectors. Data are expressed as fold change relative to the luciferase activity observed in nontransfected cells (\*\*\*\* $P < 0.0001$  by ANOVA). Experiments (G to I and K) were independently performed three times.



Downloaded from <http://stm.sciencemag.org/> at University of Science and Technology of China on April 20, 2020

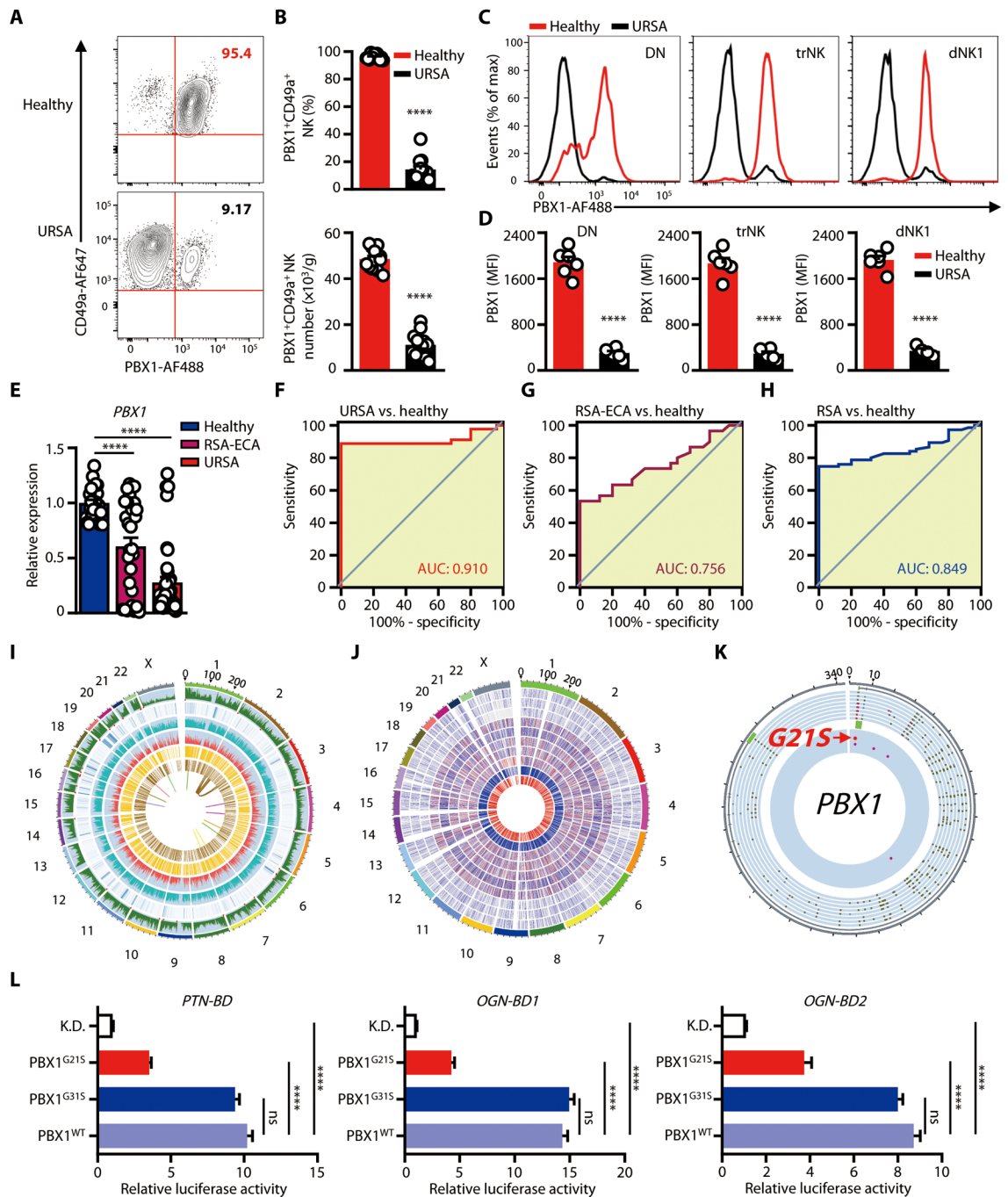
dNK cell subsets demonstrated that it was significantly decreased in CD11b<sup>+</sup>CD27<sup>-</sup> dNK double negative (DN), CD49a<sup>+</sup>EOMES<sup>+</sup> dNK (trNK), and CD39<sup>+</sup>CD49a<sup>+</sup>CD103<sup>-</sup>ITGB2<sup>-</sup> dNK (dNK1) cells from patients with URSA ( $P < 0.0001$ ; Fig. 4, C and D).

To assess *PBX1* gene expression in dNK cells from patients with recurrent spontaneous abortion (RSA), we collected 100 human de-

cidual tissue specimens, including 45 from patients with URSA, 30 from RSA patient pregnancies diagnosed with embryonic chromosomal abnormalities by copy number variation sequencing (RSA-ECA), and 25 healthy controls. Analysis of decidual tissue by qPCR showed that *PBX1* expression was significantly reduced in URSA and RSA-ECA samples compared with controls ( $P < 0.0001$ ; Fig. 4E). In addition,

**Fig. 4. Impaired PBX1 is associated with risk of URSA.**

(A and B) Representative flow cytometry of the CD49a<sup>+</sup>PBX1<sup>+</sup> NK cell subset (A) and percentage (B) (top) and number (B) (bottom) in gated CD3<sup>-</sup>CD45<sup>+</sup>CD56<sup>+</sup> dNK cells from patients with URSA (n = 12) and healthy controls (n = 12) (\*\*\*\*P < 0.0001 by two-tailed t test). (C and D) Representative flow cytometry of PBX1 expression (C) and MFI values (D) in gated CD11b<sup>-</sup>CD27<sup>-</sup> (DN), CD49a<sup>+</sup>EOMES<sup>+</sup> (trNK), and CD39<sup>+</sup>CD49a<sup>+</sup>CD103<sup>-</sup>ITGB2<sup>-</sup> (dNK) dNK cell subsets from healthy controls (red; n = 6) and patients with URSA (black; n = 6) (\*\*\*\*P < 0.0001 by two-tailed t test). (E) Quantitative RT-PCR of PBX1 in decidual tissue from first-trimester pregnancies with embryonic chromosomal abnormalities in patients with RSA (RSA-ECA; n = 30), patients with URSA (n = 45), and healthy controls (n = 25), normalized to expression in healthy decidua. (F to H) ROC curve evaluation of the relationship between decreased expression of PBX1 (E) and URSA (F), RSA-ECA (G), and RSA including URSA and RSA-ECA (H). (I to K) Plots were constructed using BioCircos.js. (I) Comprehensive catalog of whole-exome sequencing data from dNK cells from healthy controls (n = 3) and patients with URSA (n = 5). Outer ring, chromosome ideograms. From the outside inward, data tracks represent SNP density statistics (interval length, 1 million), high SNP density statistics (threshold density, >1.5), gene density statistics in the human hg19 reference genome (interval length, 1 million), average sequencing depth at each site (natural logarithm), Ts/Tv ratio (natural logarithm), type 0/1 SNP sites in the URSA group, type 1/1 SNP sites in the URSA group, and distinct fusion genes in the URSA group. (J) Plots of SNP sites in the genomes of dNK cells. Outer ring, chromosome ideograms. From the outside inward, the 1st three tracks represent SNP sites in dNK cells of healthy controls, the 4th to 8th tracks represent shared SNP sites in dNK cells from patients with URSA, the 9th track represents shared 0/1 SNP sites in dNK cells from patients with URSA, and the 10th track represents shared 1/1 SNP sites in dNK cells from patients with URSA. (K) Circular visualization of the PBX1 gene locus and SNPs within it. Outer ring, positions in the PBX1 gene. The next eight tracks are SNP sites in PBX1 in dNK cells from three healthy controls and five patients with URSA (from outside inward). The next track is exon 1 of PBX1 (length enlarged 10x). The next track shows all shared SNP sites in dNK cells from five patients with URSA, including G215 in exon 1. (L) Assay of relative luciferase activity in 293T cells with knocked down (K.D.) or WT PBX1 (PBX1<sup>WT</sup>), transfected with a vector overexpressing PBX1<sup>G215</sup> and PTN-BD or OGN-BD reporter vectors [not significant (ns), >0.05; \*\*\*\*P < 0.0001 by ANOVA]. The PBX1<sup>G215</sup> variant and WT PBX1 served as controls. Data are expressed as fold change relative to the luciferase activity observed in cells of nontransfected with reporter vectors. Experiment was independently performed three times. The numbers in (A) represent the percentages of each indicated NK subset, and those in (F) to (H) are AUC values for each ROC curve.



Downloaded from <http://stm.sciencemag.org/> at University of Science and Technology of China on April 20, 2020

*PBX1* expression was reduced in 36.7% (11 of 30) of RSA-ECA samples and 84.4% (38 of 45) of patients with URSA (Fig. 4E). Analysis of the correlation between decreased *PBX1* expression and disease using receiver operating characteristic (ROC) curves demonstrated that the area under the curve (AUC) for reduced *PBX1* expression was 0.910 [95% confidence interval (CI), 0.8338 to 0.9866] in patients with URSA (Fig. 4F). AUC values for RSA-ECA and all RSA (URSA plus RSA-ECA) were 0.756 (95% CI, 0.6281 to 0.8839) and 0.849 (95% CI, 0.7753 to 0.9217), respectively (Fig. 4, G and H).

To investigate the cause of impaired *PBX1* expression at the genetic level, we performed whole-exome sequencing of DNA from dNK cells from five patients with URSA and three healthy controls (Fig. 4I and fig. S4A). Compared with controls, dNK cell genomes of patients with URSA contained numerous single-nucleotide polymorphisms (SNPs), including shared heterozygous and homozygous SNPs (Fig. 4J, blue and red inner rings, respectively). Focusing on *PBX1*, we identified a homozygous nonsynonymous SNP, *PBX1*<sup>G21S</sup> (Fig. 4K), and Sanger sequencing of PCR amplicons from decidual tissue verified the presence of *PBX1*<sup>G21S</sup> (fig. S4, B and C).

To assess the effects of *PBX1*<sup>G21S</sup>, we overexpressed it in 293T cells with wild-type (WT) *PBX1* expression knocked down and performed functional analyses. Western blotting showed that *PBX1*<sup>G21S</sup> could bind to the *PTN* and *OGN* promoters (fig. S4D); however, luciferase assays demonstrated that *PBX1*<sup>G21S</sup> impaired activation of downstream gene expression (Fig. 4L). In addition, although *PTN* and *OGN* expression was also observed in vascular endothelial (VE) cells and a few stromal cells in decidual tissues and EVT of villous tissues (32), consistent with the flow cytometry results (fig. S5, A and B), we found prominent *PTN* and *OGN* expression in CD56<sup>+</sup> dNK cells in decidual tissue by Western blotting of extracts of purified dNK cells (fig. S5C) and multiplex immunohistochemistry staining of decidual tissues (fig. S5D). However, in decidual tissues from URSA patients with the *PBX1*<sup>G21S</sup> mutant, we found that *PTN* (red; top) and *OGN* (red; bottom) expression in CD56<sup>+</sup> dNK cells (green) was almost absent, whereas their expression did not decrease in VE cells in typical vascular structure regions (fig. S5, D and E). Furthermore, comparing the villous tissues derived from healthy controls and patients with URSA, we observed that there was no obvious difference in the expression of *PTN* (red; top) and *OGN* (red; bottom), and each of these markers was expressed in some EVT cells (fig. S5, F and G). Moreover, to evaluate the effect of reduced *GPF* expression on trophoblast cell proliferation in villus tissues from healthy controls and URSA patients with the *PBX1*<sup>G21S</sup> mutation by immunohistochemical staining to detect Ki67 and proliferating cell nuclear antigen (PCNA). Both Ki67- and PCNA-positive staining were reduced in trophoblast cells from patients with URSA, suggesting poor proliferation (fig. S5, H and I). Furthermore, color B-ultrasound data demonstrated that URSA patients with impaired *PBX1* had smaller gestational sacs relative to healthy pregnant women at similar gestational stages (fig. S5J).

### Lack of *PBX1*<sup>+</sup> dNK cells results in fetal growth restriction

To investigate the role of *PBX1* in promoting fetal growth via regulation of dNK cells, we conducted experiments in mice. An HA tag was inserted upstream of the *Pbx1* start codon to generate a *Pbx1*<sup>HA-tag</sup> knock-in mouse (fig. S6A) (33), and *PBX1* expression was evaluated by detection of the HA tag in gated NK cells from spleens and uteruses of pregnant mice at gestational day (gd) 11.5; virgin mice were

used as controls (fig. S6, B to E). *PBX1* was significantly increased in uterine NK cells from mice at gd11.5 ( $P < 0.0001$ ; fig. S6, D and E), whereas it was not expressed in spleen NK cells from gd11.5 pregnant or virgin mice (fig. S6, B and C). These data indicate that *PBX1* is expressed in NK cells at the maternal-fetal interface, rather than in pNK cells, consistent with our findings using human NK cells.

Because the amino acid sequences of human and mouse *PBX1* are completely identical, we verified *PBX1* expression in uterine NK cells from WT mice using our rat anti-*PBX1* antibody. Colabeling for CD49a, CD49b, or the transcription factors *Eomes* or T-bet revealed that the CD49a<sup>+</sup>*PBX1*<sup>+</sup> NK cell subset was increased in mouse uterus at gd11.5 (Fig. 5A). Next, to verify the role of *PBX1* in promoting fetal development through regulation of NK cells, we assessed NK cells from hematopoietic- or NK cell-specific *Pbx1*-deficient (*Pbx1*<sup>NK-KO</sup>) mice generated by crossing *Pbx1*<sup>fl/fl</sup> mice with *Vav1-Cre* or *Ncr1-Cre* mice. Intracellular flow cytometry showed that *PBX1* was knocked out in dNK cells derived from these two deficient mice (fig. S6, F and G). First, we used RNA-seq to compare gene expression in uterine NK cells from *Pbx1*<sup>fl/fl</sup>; *Ncr1*<sup>Cre</sup> mice with those in WT mice at gd11.5. Inactivation of *Pbx1* substantially altered NK cell gene expression profiles (Fig. 5B and fig. S7, A to C); specifically, we detected down-regulation of *Ptn* and *Ogn* (Fig. 5B and fig. S7B). Flow cytometric analysis of these GPFs in NK cells from *Pbx1*<sup>fl/fl</sup>; *Vav1*<sup>Cre</sup> and *Pbx1*<sup>fl/fl</sup>; *Ncr1*<sup>Cre</sup> mice verified that conditional *Pbx1* knockout in NK cells results in the near loss of *PTN* and *OGN* proteins ( $P < 0.0001$ ; Fig. 5, C to F).

Furthermore, we evaluated the role of *PBX1* in NK cells during fetal development in pregnant *Pbx1*<sup>NK-KO</sup> mice. After mating with WT male mice, female *Pbx1*<sup>fl/fl</sup>; *Vav1*<sup>Cre</sup> and *Pbx1*<sup>fl/fl</sup>; *Ncr1*<sup>Cre</sup> mice exhibited a fetal resorption phenotype (Fig. 5G), which markedly reduced the number of mice born ( $P < 0.0001$ ; Fig. 5H). Therefore, we transplanted embryos from *Pbx1* conditional knockout mice into WT surrogate mice by in vitro fertilization and found that the resulting birth rate of knockout mice was not decreased compared with that of controls (Fig. 5I). Assessment of the growth (weight and body length) of live fetuses demonstrated that those from pregnant *Pbx1*<sup>fl/fl</sup>; *Vav1*<sup>Cre</sup> and *Pbx1*<sup>fl/fl</sup>; *Ncr1*<sup>Cre</sup> mice exhibited severe fetal growth restriction, characterized by low weight, short length, and poor bone formation (Fig. 5, J to L). Staining of serial sections of intact fetuses showed that their bones contained insufficient calcium deposition and were mainly composed of cartilage that could be stained with Safranin O (fig. S7, D and E).

*Pbx1* knockout resulted in a decrease in the proportion and number of NK cells among uterine mononuclear cells from *Pbx1*<sup>fl/fl</sup>; *Vav1*<sup>Cre</sup> and *Pbx1*<sup>fl/fl</sup>; *Ncr1*<sup>Cre</sup> mice, whether pregnant or not (Fig. 6, A and B). Numbers of CD49a<sup>+</sup>*Eomes*<sup>+</sup> trNK cells were also reduced in the uteruses of *Pbx1*<sup>fl/fl</sup>; *Vav1*<sup>Cre</sup> and *Pbx1*<sup>fl/fl</sup>; *Ncr1*<sup>Cre</sup> mice (Fig. 6, C and D). Therefore, we speculated that *PBX1* may affect NK cell proliferation. Hence, we evaluated Ki67 expression to assess the proliferative capacity of NK cells. There were fewer Ki67<sup>+</sup> NK cells in both *Pbx1*<sup>fl/fl</sup>; *Vav1*<sup>Cre</sup> and *Pbx1*<sup>fl/fl</sup>; *Ncr1*<sup>Cre</sup> mice, indicating that *PBX1* can maintain NK cell number stability at the maternal-fetal interface (Fig. 6, E and F). Carboxyfluorescein diacetate succinimidyl ester (CFSE) and bromodeoxyuridine (BrdU) labeling assays further confirmed the effect of *PBX1* on the proliferation ability of dNK cells (Fig. 6, G to I). Hence, *PBX1* both regulates NK cells' proliferative capacity and promotes their expression of GPFs.

In addition, we found that, although uterine CD49a<sup>+</sup>*Eomes*<sup>+</sup> trNK cells were not detected in *Eomes*<sup>fl/fl</sup>; *Ncr1*<sup>Cre</sup> mice (Fig. 6, C and D),

**Fig. 5. Fetal growth restriction in pregnant *Pbx1*<sup>NK</sup> knockout mice is due to decreased expression of GPFs.** (A) Representative flow cytometry of PBX1<sup>+</sup> NK cell subsets colabeled with CD49a, CD49b, Eomes, and T-bet in gated CD3<sup>+</sup>CD45<sup>+</sup>NK1.1<sup>+</sup> NK cells from mouse uterus at gd11.5, with virgin mice as controls. (B) Differential analysis of gene expression based on RNA-seq data from uterine NK cells from *Pbx1*<sup>fl/fl</sup>;Ncr1<sup>Cre</sup> and *Pbx1*<sup>fl/fl</sup> mice at gd11.5. (C and D) Intracellular flow cytometric analysis of PTN and OGN expression in NK cells from *Pbx1*<sup>fl/fl</sup>;Vav1<sup>Cre</sup> (C) and *Pbx1*<sup>fl/fl</sup>;Ncr1<sup>Cre</sup> (D) mice. *Pbx1*<sup>fl/fl</sup> mice served as the control group. IgG antibody, negative control. (E and F) Statistical analysis of the relative MFI values for PTN and OGN in NK cells from *Pbx1*<sup>fl/fl</sup>;Vav1<sup>Cre</sup> (E) and *Pbx1*<sup>fl/fl</sup>;Ncr1<sup>Cre</sup> (F) mice (*n* = 6), normalized to MFI in negative control (\*\*\*\**P* < 0.0001 by two-tailed *t* test). (G) Representative photographs of fetuses from *Pbx1*<sup>fl/fl</sup>;Vav1<sup>Cre</sup> and *Pbx1*<sup>fl/fl</sup>;Ncr1<sup>Cre</sup> at gd16.5 and gd19.5. Scale bar, 5 mm. E16.5, embryonic day 16.5. (H) Statistical analysis of the number of live fetuses from *Pbx1*<sup>fl/fl</sup>;Vav1<sup>Cre</sup> and *Pbx1*<sup>fl/fl</sup>;Ncr1<sup>Cre</sup> pregnant female mice (*n* = 15) mated with B6 male mice. (I) Statistical analysis of the birth rates of WT surrogate mice carrying heterozygous *Pbx1*<sup>fl/fl</sup>;Vav1<sup>Cre</sup> and *Pbx1*<sup>fl/fl</sup>;Ncr1<sup>Cre</sup> embryos from female knockout mice (*n* = 4) mated with B6 male mice by in vitro fertilization (IVF). (J) Representative photographs of skeletal staining of embryos (gd16.5 and gd19.5) from *Pbx1*<sup>fl/fl</sup>;Vav1<sup>Cre</sup> and *Pbx1*<sup>fl/fl</sup>;Ncr1<sup>Cre</sup> pregnant female mice. Scale bars, 2 mm. (K and L) Statistical analyses of the average weight (K) and body length (L) of fetuses (gd16.5 and gd19.5) from *Pbx1*<sup>fl/fl</sup>;Vav1<sup>Cre</sup> and *Pbx1*<sup>fl/fl</sup>;Ncr1<sup>Cre</sup> mice. The numbers in (A) are the percentage of each indicated NK subset, and those in (C) and (D) are the MFI for each GPF. Experiments (A, C, D, G, I, and J) were independently performed three times, and statistical analyses (H, I, K, and L) were conducted by ANOVA (ns, >0.05; \**P* < 0.05, \*\*\**P* < 0.001, and \*\*\*\**P* < 0.0001).

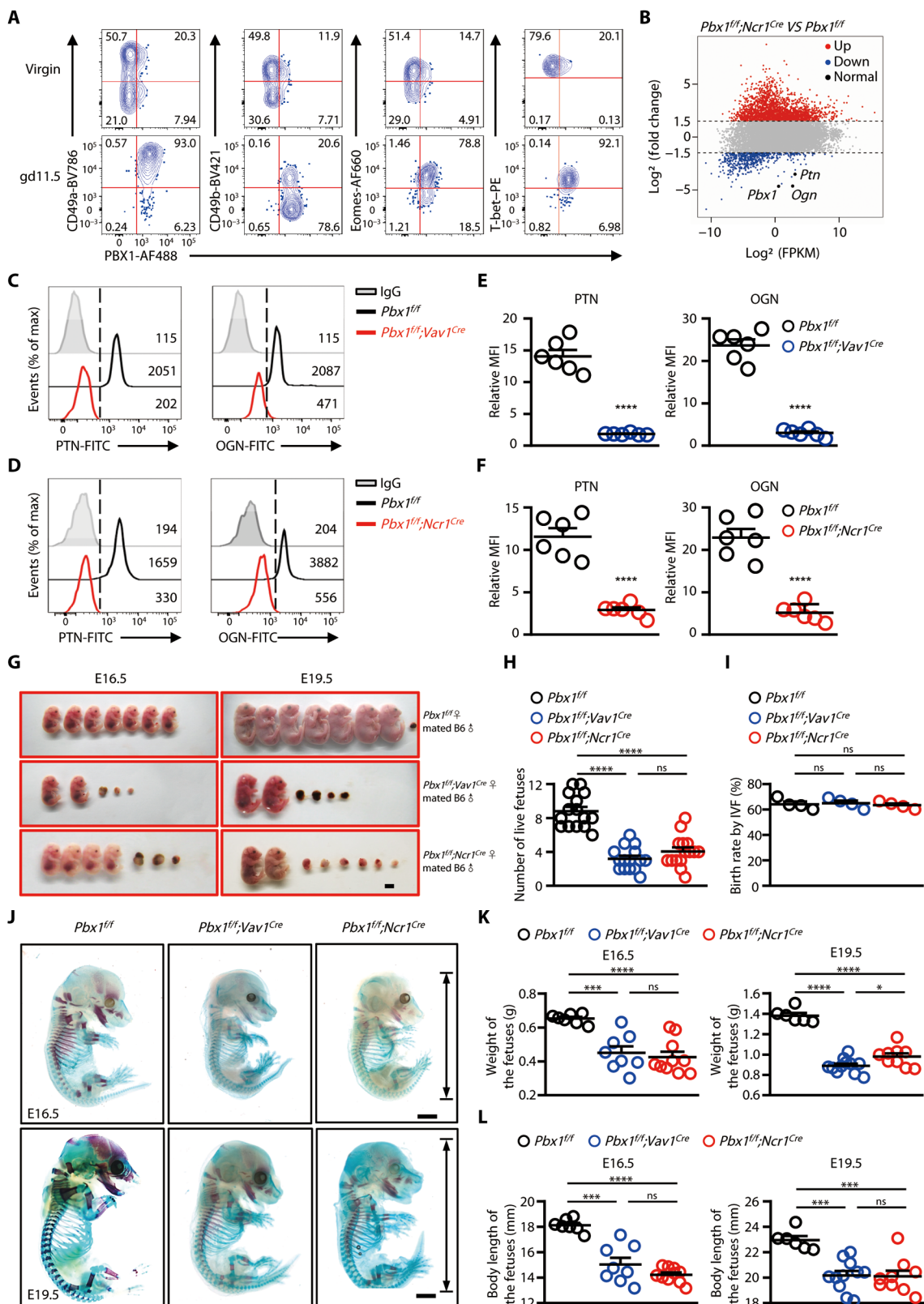
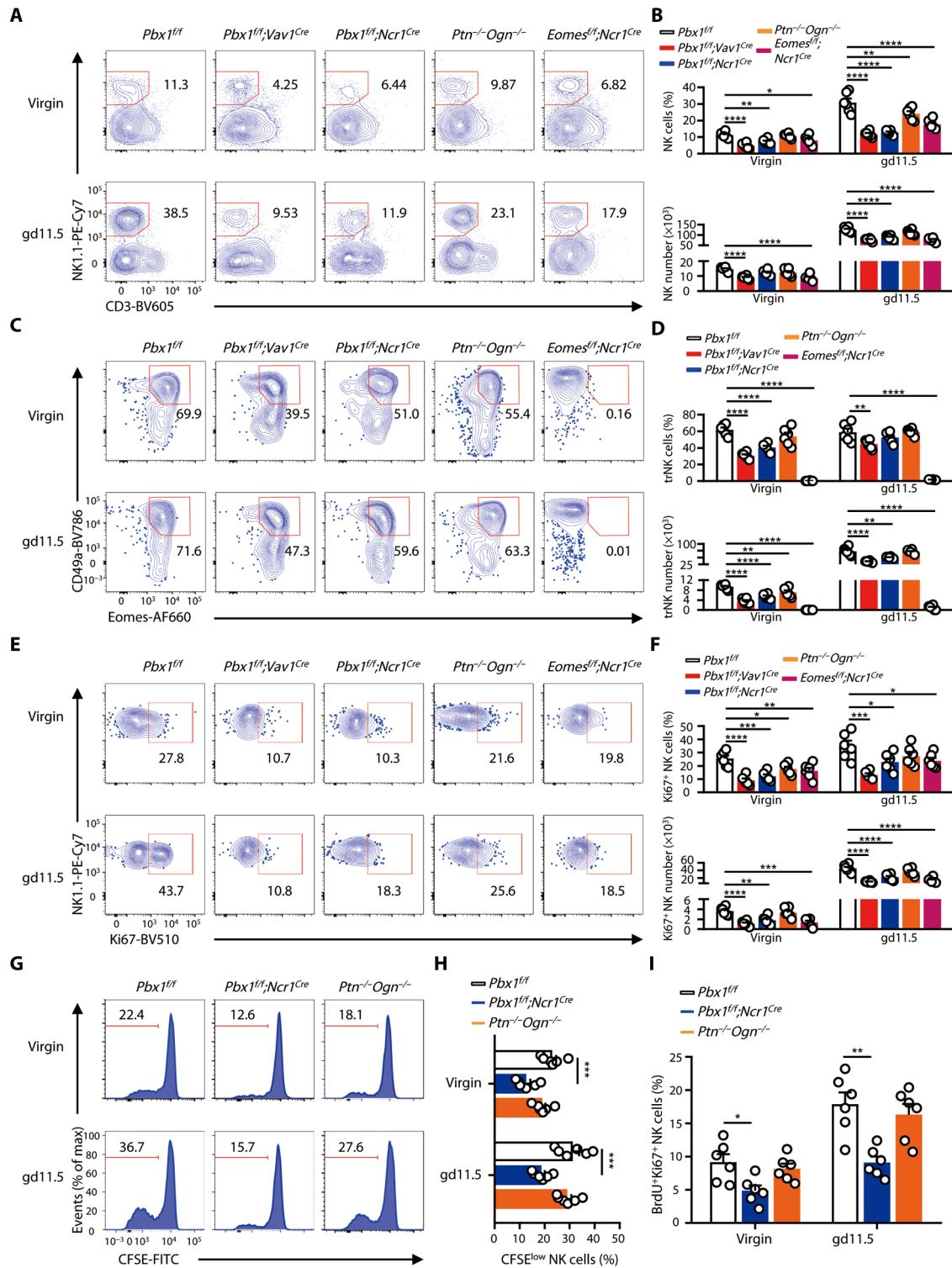


**Fig. 6. Decreased numbers of uterine trNK cells in *Pbx1*<sup>NK-KO</sup> mice.**

**(A)** Representative flow cytometry of CD3<sup>-</sup>NK1.1<sup>+</sup> NK cells in uterine tissue from *Pbx1*<sup>fl/fl</sup>, *Pbx1*<sup>fl/fl</sup>;*Vav1*<sup>Cre</sup>, *Pbx1*<sup>fl/fl</sup>;*Ncr1*<sup>Cre</sup>, *Ptn*<sup>-/-</sup>*Ogn*<sup>-/-</sup>, and *Eomes*<sup>fl/fl</sup>;*Ncr1*<sup>Cre</sup> mice at gd11.5 and virgin mice as controls. **(B)** Statistical analysis of percentages (top) and numbers (bottom) of cells in each indicated subset in (A). **(C)** Representative flow cytometry of CD49a<sup>+</sup>*Eomes*<sup>+</sup> trNK cells in uterine tissue from the indicated mice. **(D)** Statistical analysis of percentages (top) and numbers (bottom) of cells in each indicated subset in (C). **(E)** Representative flow cytometry of Ki67<sup>+</sup> NK cells in uterine tissue from the indicated mice. **(F)** Statistical analysis of percentages (top) and numbers (bottom) of cells in each indicated subset in (E). **(G and H)** Representative flow cytometry (G) and statistical percentages (H) of CFSE<sup>+</sup> NK cells in uterine tissue from *Pbx1*<sup>fl/fl</sup>, *Pbx1*<sup>fl/fl</sup>;*Ncr1*<sup>Cre</sup>, and *Ptn*<sup>-/-</sup>*Ogn*<sup>-/-</sup> mice at gd11.5. **(I)** Statistical analysis of percentages of BrdU<sup>+</sup>Ki67<sup>+</sup> NK cells in uterine tissue from the indicated mice. The numbers in (A), (C), (E), and (G) represent the percentages of the indicated subsets. Statistical analyses were conducted using data from all biological replicates (*n*=6) by ANOVA (\*\**P*<0.05, \*\*\**P*<0.01, \*\*\*\**P*<0.0001), and all experiments were performed three times.



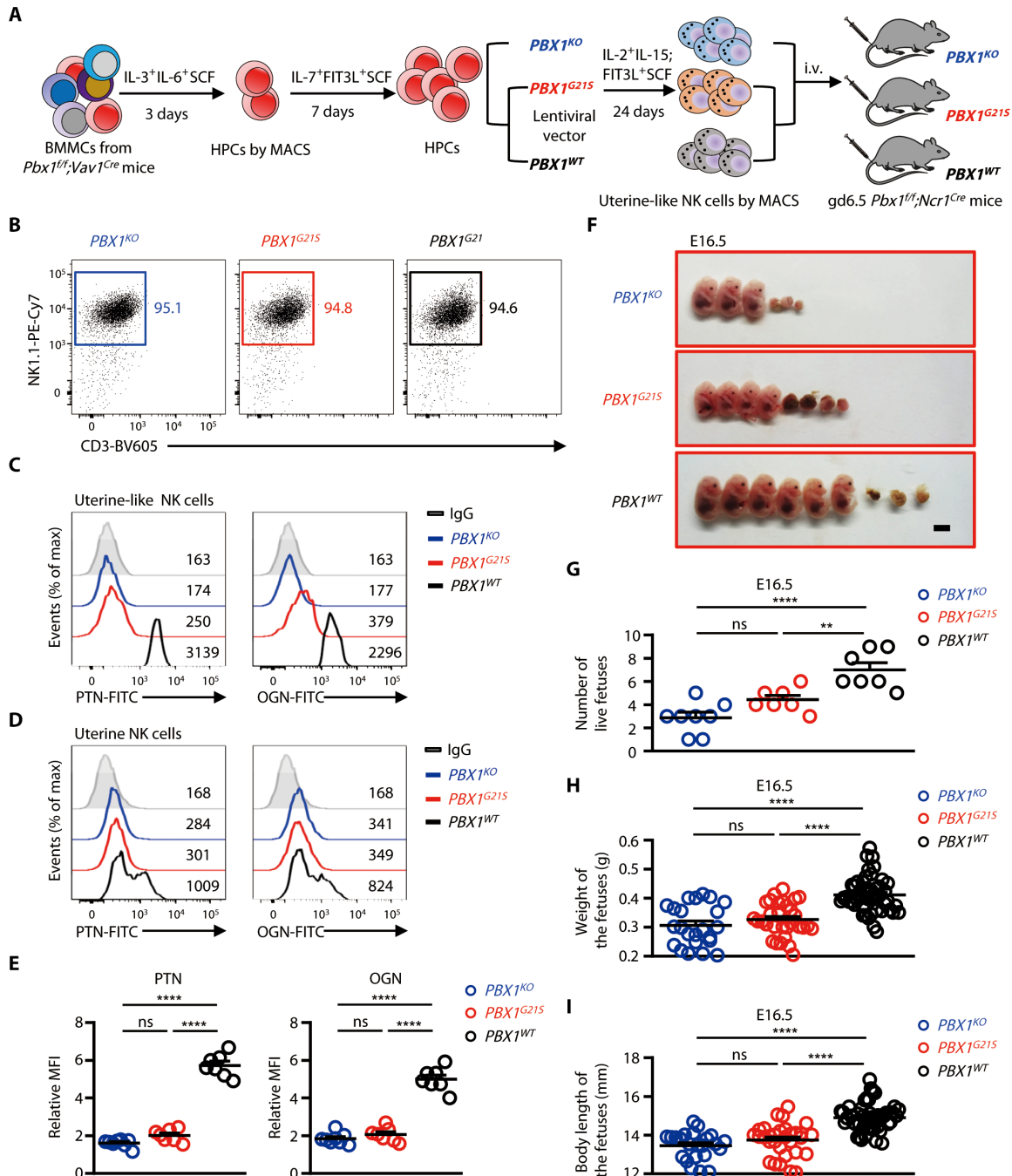
the developmental status of the offspring was similar to that of controls (fig. S8). These data further confirm the function of PBX1 in promoting fetal development via NK cells at the maternal fetal interface in both humans and mice.

**Transfer of uterine-like NK cells with PBX1<sup>WT</sup> rescues fetal growth**

PBX1<sup>G21S</sup> was identified in dNK cells from patients with URSA as a mutation that impairs the transcriptional regulation of *PTN* and

*OGN* by PBX1. To determine whether transfer of PBX1<sup>G21S</sup> overexpressing NK cells could restore normal pregnancy in *Pbx1*<sup>fl/fl</sup>;*Ncr1*<sup>Cre</sup> mice, we used a previously reported in vitro induction system of mouse uterine-like NK cells (11). The *Pbx1*<sup>fl/fl</sup>;*Vav1*<sup>Cre</sup> mouse is a model where *Pbx1* becomes defective in hematopoietic progenitor cells, so bone marrow precursor cells from the mouse were induced

**Fig. 7. Uterine-like NK cells expressing PBX1<sup>WT</sup> rescue pregnancy in *Pbx1*-CKO mice. (A)** Schematic representation of the in vitro cell system for induction of uterine-like *Pbx1*-deficient (PBX1<sup>KO</sup>) NK cells by expressing PBX1<sup>G21S</sup> or PBX1<sup>WT</sup> for transferring into *Pbx1<sup>fl/fl</sup>;Ncr1<sup>Cre</sup>* pregnant female mice. i.v., intravenous. (B) Representative flow cytometry data showing the percentage of CD3<sup>+</sup>NK1.1<sup>+</sup> uterine NK cells from uterine-like NK cells after purification. (C and D) Intracellular flow cytometric analysis of PTN and OGN expression in uterine-like NK cells before transfusion (C) and dNK cells after transfusion (D) from *Pbx1<sup>fl/fl</sup>;Ncr1<sup>Cre</sup>* pregnant mice. IgG antibody, negative control. (E) Statistical analysis of the relative MFI values for PTN and OGN in dNK cells shown in (D), normalized to MFI in negative control (\*\*\*\**P* < 0.0001 by ANOVA). (F) Representative photographs of fetuses from *Pbx1<sup>fl/fl</sup>;Ncr1<sup>Cre</sup>* mice transfected with PBX1<sup>KO</sup>, PBX1<sup>G21S</sup>, and PBX1<sup>WT</sup> NK cells at gd16.5. Scale bar, 5 mm. (G) Statistical analysis of the number of live fetuses from *Pbx1<sup>fl/fl</sup>;Ncr1<sup>Cre</sup>* mice transfected with PBX1<sup>KO</sup> (*n* = 8), PBX1<sup>G21S</sup> (*n* = 7), and PBX1<sup>WT</sup> (*n* = 7) NK cells at gd16.5 (\*\**P* < 0.01 and \*\*\*\**P* < 0.0001 by ANOVA). (H and I) Statistical analyses of the weight (H) and body length (I) of fetuses (gd16.5) from *Pbx1<sup>fl/fl</sup>;Ncr1<sup>Cre</sup>* mice transfected with PBX1<sup>KO</sup> (*n* = 8), PBX1<sup>G21S</sup> (*n* = 7), and PBX1<sup>WT</sup> (*n* = 7) NK cells (\*\*\*\**P* < 0.0001 by ANOVA). The numbers in (B) are the percentage of each indicated NK subset, and those in (C) and (D) are the MFI for each GFP. Statistical analyses were conducted using data from two independent experiments with similar results.



to develop into uterine-like NK cells using a cytokine cocktail lack PBX1. The expression of PBX1<sup>WT</sup> or PBX1<sup>G21S</sup> mutant can be restored using a lenticral vector, and cells can then be purified to obtain uterine-like NK cells with PBX1<sup>KO</sup>, PBX1<sup>G21S</sup>, or PBX1<sup>WT</sup> for transfer to *Pbx1<sup>fl/fl</sup>;Ncr1<sup>Cre</sup>* mice at gd6.5 (Fig. 7, A and B). Uterine-like NK cells overexpressing PBX1<sup>WT</sup>, but not PBX1<sup>G21S</sup>, restored PTN and OGN expression (Fig. 7C). Furthermore, dNK cells expressing growth factors were also detected in mouse uterine tissue after transfer of PBX1<sup>WT</sup>, but not PBX1<sup>G21S</sup>, overexpressing uterine-like

NK cells (Fig. 7, D and E). To evaluate the pregnancy quality of *Pbx1<sup>fl/fl</sup>;Ncr1<sup>Cre</sup>* mice after cell transfer at gd16.5, we assessed both the number of live fetuses (*P* < 0.0001 and *P* = 0.0039; Fig. 7, F and G) and their weight (*P* < 0.0001 and *P* = 0.3843; Fig. 7H) and length (*P* < 0.0001 and *P* = 0.2490; Fig. 7I). Fetuses exhibited significant restoration after transfer of PBX1<sup>WT</sup>, but not PBX1<sup>G21S</sup>, overexpressing uterine-like NK cells. These findings once again demonstrate that the PBX1<sup>G21S</sup> mutant in dNK cells, while not affecting the ability of PBX1 to bind to its target gene promoters, impairs promotion

of *Ptn* and *Ogn* transcription, resulting in fetal growth restriction in mice.

## DISCUSSION

Various transcription factors, including T-bet and Eomes, have been investigated on classical NK cells connected with their cytotoxic and regulatory functions (34–36). Here, we identified PBX1 as a distinct functional transcription factor in dNK cells that promote fetal development via up-regulating the expression of GPFs (fig. S9). Clinically, we suggest that NK cell dysfunction, caused by impaired PBX1, is potentially an important contributor to URSA pathogenesis and may be a useful diagnostic indicator.

There are a variety of NK cell subsets that perform important functions at the maternal-fetal interface (4, 5). In human and mouse models, we have shown that CD49a<sup>+</sup>EOMES<sup>+</sup> NK cells with a trNK cell phenotype in uterine tissue can directly produce GPFs that nourish fetal development before the placenta can provide adequate nutrition (11); however, we did not observe GPFs reduction and fetal growth restriction in *Eomes<sup>f/f</sup>;Ncr1<sup>Cre</sup>* mice, suggesting that the transcription factor EOMES may be a signature for uterine trNK cells but may not be critical for the functional subsets that promote fetal growth. Focusing on transcription factor array data from human dNK cells, we identified the transcription factor PBX1, expressed both in the CD49a<sup>+</sup>EOMES<sup>+</sup> and CD11b<sup>-</sup>CD27<sup>-</sup> NK cell subsets that produce GPFs to promote fetal development.

PBX1 is a transcription factor with important roles in the embryonic development of multiple organs, including skeletal bone and neuronal and cardiovascular differentiation (37–39). Our data show that PBX1 can directly bind to the promoters of the GPFs *PTN* and *OGN* in dNK cells from pregnant women and mice to promote their transcription. Meanwhile, decreased dNK cell numbers have been observed in two mouse models of *Pbx1<sup>NK</sup>-KO* mediated by *Vav1<sup>Cre</sup>* and *Ncr1<sup>Cre</sup>*. Furthermore, we have shown that PBX1 is predominantly expressed in CD49a<sup>+</sup> trNK cells. Although bone marrow-derived CD27<sup>low</sup>CD49b<sup>+</sup> NK cells are important for successful pregnancy in both mice and humans (40), uterine tissue contains few circulating conventional CD27<sup>low</sup>CD49b<sup>+</sup> NK cells, whereas CD27<sup>low</sup>CD49a<sup>+</sup> trNK cells are abundant in both mouse and human decidua (4, 11, 15, 31). Although our results suggest that the reduced numbers of uterine NK cells in *Pbx1<sup>NK</sup>-KO* mice are mainly related to the decreased cell proliferation, target genes of PBX1 involved in cell proliferation regulation have not been found, suggesting that PBX1 may indirectly modulate this process. It seems that PBX1 has a dual function as a transcription factor in affecting cell proliferation and regulating expression of GPFs in dNK cells, with enhancement of GPFs occurring through a more direct mechanism. Moreover, we elucidate the regulatory mechanism upstream of PBX1, in which EVT-derived HLA-G promotes activation of AKT1 in dNK cells by interacting with ILT2, thereby driving the expression of PBX1.

The mechanism of how GPFs affect fetal growth still needs more investigations. One possibility is that GPFs may promote fetal growth through affecting spiral artery remodeling at the maternal-fetal interface, which has been listed as one of the main functions of dNK cells (22, 23, 41). Another possibility is that these GPFs may also induce the development and function of dNK cells themselves, for decreased numbers of dNK cells have been observed in *Pbx1<sup>NK</sup>-KO* mice. It is notable that impaired PBX1 in dNK cells is associated

with URSA. However, more data in larger clinical cohort studies are needed to confirm the value of PBX1 in the diagnosis and treatment of patients with URSA.

The cause of recurrent miscarriage is difficult to pinpoint in half of the patients, resulting in a clinical diagnosis of URSA (12, 14). Genetic screening of embryonic chromosomes has become a common method for diagnosis of RSA (42); however, the lack of indicators for evaluation of endometrial immune cells has long been problematic. Here, we show that the CD49a<sup>+</sup>PBX1<sup>+</sup> dNK cell subset is reduced in patients with URSA and that decreased PBX1 expression in the dNK cells has potential to predict disease occurrence. Moreover, we identified the PBX1<sup>G21S</sup> mutant, which results in loss of PBX1 transcription regulation activity in dNK cells from some patients with URSA, and confirmed that the PBX1<sup>G21S</sup> mutant cannot drive expression of GPFs, resulting in fetal growth restriction, through the cell transfer model of uterine-like NK cells overexpressing PBX1<sup>G21S</sup>. Therefore, we speculate that decreased PBX1 expression or PBX1<sup>G21S</sup> mutant may be associated with increased risk of RSA, particularly URSA.

In summary, our data reveal that the transcription factor PBX1 drives uterine NK cells to promote fetal development by up-regulating the expression of GPFs. These findings indicate that impaired CD49a<sup>+</sup>PBX1<sup>+</sup> NK cells contribute to the etiology of URSA, with potential value for clinical diagnosis.

## MATERIALS AND METHODS

### Study design

This study aimed to explore the key transcription factor and the mechanisms that regulate GPFs in CD49a<sup>+</sup> trNK cells from decidual tissues of healthy women and patients with URSA. We addressed this objective by (i) developing a monoclonal antibody showing that PBX1 is expressed in dNK cells from human and mice, (ii) demonstrating that the HLA-G-ILT2-AKT axis drives PBX1 expression that can promote transcription of GPFs based on the results of dNK cell antibody microarray and ChIP-seq, and (iii) revealing that impaired PBX1 in dNK cells may be associated with increased risk of URSA based on the results of PBX1 protein of dNK cells from patients with URSA and the phenotype of *Pbx1<sup>NK</sup>-KO* mice and mouse transfer model of uterine-like NK cells with PBX1<sup>G21S</sup> mutant. Investigators were not blinded to group identity.

Fresh decidual samples (table S1) were obtained from pregnancies ( $n = 45$ ) that were voluntarily terminated or from patients with pregnancy complications ( $n = 20$ ), including recurrent spontaneous abortions where embryos had normal karyotypes. Abortions due to genetic abnormalities detected by chorionic villus sampling or anatomical examination were excluded. Fresh decidual samples were derived from healthy donors and patients at the First Affiliated Hospital of the University of Science and Technology of China. Cryopreserved decidual samples (table S1) were obtained from patients who experienced recurrent spontaneous abortions with no embryonic chromosomal abnormalities (ECAs) ( $n = 45$ ) or with ECAs ( $n = 30$ ). Cryopreserved decidual samples were derived from patients at the First Affiliated Hospital of the Zhengzhou University. Echo sonography was performed every 2 weeks, and patients were advised to undergo induced abortion if the fetal heartbeat was not detected or had stopped. Fetal heartbeat was determined before voluntary termination among pregnant women with no history of

miscarriage. Before surgery, informed consent was obtained from each patient. Umbilical cord blood samples were from healthy donors at the First Affiliated Hospital of the University of Science and Technology of China. Peripheral blood from healthy donors was collected from the Blood Center of Anhui Province. Sample sizes were dependent on sample availability and were not predetermined. Ethical approvals were obtained from the Ethics Committee of the University of Science and Technology of China.

*Pbx1<sup>ff</sup>* mice were a gift from X. Zhang and N. Shen (Institute of Health Sciences, Chinese Academy of Sciences). *Vav1<sup>Cre</sup>*, *Ncr1<sup>Cre</sup>*, and *Eomes<sup>ff</sup>;Ncr1<sup>Cre</sup>* mice were a gift from Z. Dong (Tsinghua University). To generate the *Pbx1* deletion in NK cells, *Pbx1<sup>ff</sup>* mice were crossed with *Vav1<sup>Cre</sup>* or *Ncr1<sup>Cre</sup>* mice to obtain *Pbx1<sup>ff</sup>;Vav1<sup>Cre</sup>* or *Pbx1<sup>ff</sup>;Ncr1<sup>Cre</sup>*. To generate *Ptn<sup>-/-</sup>Ogn<sup>-/-</sup>* mice, *Ptn<sup>-/-</sup>Ogn<sup>-/-</sup>Spp1<sup>-/-</sup>* mice were crossed with WT mice. All mice used were C57BL/6, 8 to 12 weeks of age, and housed under specific pathogen-free conditions with approval from the ethics committee of the University of Science and Technology of China. All mice were studied in groups assembled based on genotype. All experimental animal procedures were conducted in accordance with the National Guidelines for Animal Usage in Research (China).

### Cell line

Human embryonic kidney 293T cells from The Cell Bank of Type Culture Collection of Chinese Academy of Sciences, Shanghai, China, were cultured in complete Dulbecco's modified Eagle's medium supplemented with 10% fetal bovine serum (HyClone) plus 1% streptomycin and penicillin at 37°C.

### Cell preparation and purification

NK cells were isolated from decidual samples and peripheral blood as follows: Briefly, mononuclear cells were extracted from decidual samples after digestion with collagenase type IV and preparation of peripheral blood samples by density gradient centrifugation through Ficoll. Purification of NK cells from decidual mononuclear cells requires adherent culture overnight to remove stromal cells. NK cells were further purified by negative selection using a magnetic-activated cell sorter (MACS) kit (Miltenyi Biotec) or by sorting using a FACSAria II cytometer (BD Biosciences). Umbilical cord blood CD34<sup>+</sup> stem cells were prepared as follows: Briefly, mononuclear cells from cord blood were prepared by density gradient centrifugation through Ficoll, and then CD34<sup>+</sup> stem cells were purified by positive selection using a MACS kit (Miltenyi Biotec). Commercial kits are listed in table S2.

### Differentiation of the decidual-like NK cell in vitro model

For in vitro induction of decidual-like NK cells from human cord blood hematopoietic stem cells, purified CD34<sup>+</sup> cells were cultured in GMP Serum-free Stem Cell Growth Medium (CellGro/CellGenix) supplemented with 10% fetal bovine serum (Gibco), stem cell factor (SCF) (20 ng/ml), Flt3L (30 ng/ml), and interleukin-15 (IL-15) (20 ng/ml). Plates were incubated for 5 weeks at 37°C in a humidified atmosphere with 5% CO<sub>2</sub>. Half of the medium was removed and replaced with fresh medium and cytokines twice every week.

Murine uterine-like NK cells were induced in vitro using hematopoietic precursor cells (HPCs) from *Pbx1<sup>ff</sup>;Vav1<sup>Cre</sup>* mouse bone marrow, as previously described (11). 5-Fluorouracil (Sigma-Aldrich) was administered to mice by intraperitoneal injection at 200 mg/kg body weight to enrich HPCs 4 days before collection of bone marrow

cells. Recombinant murine SCF (50 ng/ml), IL-6 (10 ng/ml), and IL-3 (6 ng/ml) were used to induce HPC proliferation. The expanded cells were purified using a lineage cell depletion kit (Miltenyi Biotec). One week after supporting culture with SCF (5 ng/ml), Flt3L (5 ng/ml), and IL-7 (5 ng/ml), PBX1<sup>G21S</sup> or PBX1<sup>WT</sup> was overexpressed in *Pbx1*-deficient cells using the pCDH-puro lentiviral vector. Lentivirus-infected cells were cultured to support uterine-like NK cells expressing PBX1<sup>G21S</sup> and PBX1<sup>WT</sup> for 24 days in puromycin (1 µg/ml), SCF (5 ng/ml), Flt3L (5 ng/ml), IL-2 (200 UI/ml), and IL-15 (30 ng/ml) in Iscove's modified Dulbecco's medium. After completion of the culture, the expression of GFPs was analyzed, and uterine-like NK cells were obtained by purification using phycoerythrin (PE)-anti-NKp46 antibody and anti-PE microbeads (Miltenyi Biotec). These purified induced uterine-like NK cells expressing PBX1<sup>KO</sup>, PBX1<sup>G21S</sup>, and PBX1<sup>WT</sup> were collected, washed, and prepared for adoptive transfer. Recombinant proteins are listed in table S3.

### Adoptive transfer of uterine-like NK cells

C57BL/6 male mice were randomly assigned to mate with *Pbx1<sup>ff</sup>;Ncr1<sup>Cre</sup>* female mice, and the timing of detection of a copulation plug was regarded as gd0.5. Purified uterine-like NK cells expressing PBX1<sup>KO</sup>, PBX1<sup>G21S</sup>, and PBX1<sup>WT</sup> were transferred to *Pbx1<sup>ff</sup>;Ncr1<sup>Cre</sup>* mice at 6.5 days gestation through the tail vein [1 × 10<sup>6</sup> cells/200 µl of phosphate-buffered saline (PBS) per mouse]. At 16.5 days of gestation, the three groups of recipient mice were euthanized, and uterine NK cells were isolated for detection of GFP expression and assessment of fetus number, weight, and body length.

### Flow cytometry assay

Human and mouse monoclonal antibodies (table S4) were used for measurement of cell surface markers. Matched immunoglobulin G (IgG) or IgM antibodies were used as isotype controls. For intracellular staining of transcription factors and GFPs, cells were collected by surface staining and then treated with Permeabilization Buffer from the Foxp3 Transcription Factor Staining Buffer Set (eBioscience) according to the manufacturer's instructions. Flow cytometry was performed using BD LSR II or BD LSRFortessa instruments (BD Biosciences) according to the manufacturer's instructions. Cell sorting was conducted using a FACSAria II cytometer (BD Biosciences). Data were analyzed using FlowJo vX.0.7 software (Tree Star).

### Assay for uterine NK cell proliferation in vitro

After the mouse uterus tissue was digested with collagenase IV, mononuclear cells were obtained by density gradient centrifugation through Percoll. Mouse uterine mononuclear cells (1 × 10<sup>6</sup> cells/ml PBS) were labeled with 2.5 mM CFSE (Sigma-Aldrich) for 10 min at 37°C. In another method, 1 mM BrdU solution (BrdU Flow Kit, BD Biosciences) was added to the complete medium of mouse uterus mononuclear cells (1 × 10<sup>6</sup> cells/ml), and BrdU was incorporated into the cells during proliferation. The labeled mouse uterus mononuclear cells were cultured in RPMI1640 complete medium with IL-15 (30 ng/ml) for 24 hours. The cells were then harvested, fluorescent antibody staining including CD3, CD45, NK1.1, Ki67, and BrdU was performed according to the FITC BrdU Flow Kit (BD Biosciences) instructions, and CD3<sup>-</sup>CD45<sup>+</sup>NK1.1<sup>+</sup> NK cells were assayed for CFSE dilution or the percentage of BrdU<sup>+</sup>Ki67<sup>+</sup> cells to evaluate the proliferation ability of mouse uterine NK cells.

**qPCR assays**

dNK-like cells were harvested or purified using the in vitro induction system. Cryopreserved decidual tissue samples from patients who experienced recurrent spontaneous abortions, with or without ECAs, were lysed in liquid nitrogen. Total RNA was extracted using TRIzol reagent (Invitrogen) and glycogen (Invitrogen), then 10% sodium acetate (Invitrogen), and an equal volume of precooled isopropanol was added to extracted RNA supernatants. After mixing, RNA was precipitated overnight at  $-80^{\circ}\text{C}$ . Next, complementary DNA was synthesized using M-MLV Reverse Transcriptase (Invitrogen), and qPCR was performed using SYBR Premix Ex Taq (TaKaRa) with a LightCycler 96 instrument (Roche). The  $2^{-\Delta\Delta\text{Ct}}$  method was used to analyze the resulting data. Target gene primers are listed in table S5.

**Signaling pathway antibody microarray**

Human dNK cells freshly isolated using the NK MACS kit (Miltenyi Biotec) were divided into two parts, one of which was cocultured with corresponding EVT cells for 48 hours. Subsequently,  $5 \times 10^6$  dNK cells and dNK cells cocultured with EVT cells were purified separately by sorting. Signaling pathways in purified dNK cells were analyzed using a Cell Signaling Profiling Plus (CSP100 Plus) antibody microarray (Wayne Biotechnologies).

**Western blotting**

To detect the expression of transcription factors and AKT pathway, cells were harvested and lysed on ice in radioimmunoprecipitation assay buffer containing a protease inhibitor cocktail (TransGen), and supernatants were collected by centrifugation. Protein concentrations were determined spectrophotometrically. Equal amounts of protein were separated by SDS-polyacrylamide gel electrophoresis and transferred to polyvinylidene difluoride (PVDF) membranes, followed by probing with antibody. Antibodies used for Western blotting are listed in table S4. Immunoreactive protein bands were visualized by chemiluminescence autoradiography. After the detection of phosphorylated AKT on the PVDF membrane, the labeled primary antibody and secondary antibody were washed away using Stripping Buffer (Beyotime), and it was reused to detect the expression of AKT1 protein. AKTi-1/2 is a classic AKT kinase inhibitor (Merck, cat. no. 612847-09-3).

**siRNA interference**

Synthesis of siRNA-*PBX1*, siRNA-*PKD2*, siRNA-*AKT1*, or siRNA-*NC* (table S6) was conducted by GenePharma. Nucleofector technology was used to transfect siRNA into primary human dNK cells, using a Human NK Cell Nucleofector Kit (VPA-1005, Lonza), followed by coculturing with EVT for 48 hours. Transfected dNK cells were purified using anti-CD56 MACS sorting, followed by qPCR or Western blotting analysis.

**ChIP assay**

ChIP analysis of the transcription factor PBX1 in dNK cells was performed using a ChIP assay kit (Millipore) and a standardized protocol. After cells were cross-linked using 1% formaldehyde (Invitrogen), chromatin was sheared by sonication. Equal amounts (10 mg) of rabbit anti-PBX1 antibody or control rabbit IgG (Cell Signaling Technology) were used to immunoprecipitate cross-linked DNA/protein complexes. An equal amount (10 mg) of anti-HA tag (TransGen) was used to precipitate cross-linked DNA/protein

complexes from expanded murine NK cells. After de-cross-linking, antibody-enriched purified chromatin was used for sequencing or PCR analysis. ChIP-seq binding peak results were normalized to those from the IgG group. ChIP-seq data were deposited in the Gene Expression Omnibus (GEO) database repository with the accession number GSE110244. PCR primers were designed for specific target regions and are listed in table S7.

**Promoter reporter assay and PBX1 pull-down**

Putative PBX1-binding domains in the *PTN* and *OGN* promoters were amplified and inserted into pGL3-based luciferase reporter plasmids, followed by transfection into 293T cells. After 48 hours of transfection, 5 million cells were collected, and luciferase activity was detected using a Dual-Luciferase Reporter Assay System (Promega) according to the manufacturer's protocol. Putative PBX1-binding site sequences in the *PTN* and *OGN* promoter regions were synthesized as biotinylated probes. 293T cell nucleoprotein lysates were collected and incubated with streptavidin microbeads (Miltenyi Biotec) in the presence or absence of the biotinylated probes for 4 hours at  $4^{\circ}\text{C}$ . Pulldown elution products were analyzed by Western blotting.

**Whole-exome sequencing**

Genomic DNA was extracted from purified  $\text{CD3}^{-}\text{CD45}^{+}\text{CD56}^{+}$  NK cells from three healthy controls and five patients with URSA for whole-exome sequencing analysis. Libraries were constructed by Hybrid Selection and sequenced using the HiSeq X Ten platform (Illumina). Human hg19 (GRCh37) was used as the reference genome, and NK cells from healthy individuals served as controls. Whole-exome sequencing data were deposited in the Sequence Read Archive (SRA) database repository: BioProject PRJNA517620 (SRA: SRR8505897-8505904).

**RNA-seq assay**

Differential analysis of gene expression profiles in uterine NK cells from *Pbx1<sup>fl/fl</sup>* and *Pbx1<sup>fl/fl</sup>; Ncr1<sup>Cre</sup>* mice at gd11.5 was performed in duplicate by deep sequencing using the Illumina HiSeq X Ten platform.  $\text{CD3}^{-}\text{CD45}^{+}\text{NK1.1}^{+}$  NK cells were sorted from mouse uterine tissue. Total RNA was extracted and purified using an miRNeasy Mini Kit (Qiagen) and treated with RNase-Free DNase. RNA libraries were prepared for sequencing using standard Illumina protocols. Adaptor sequences were trimmed from sequenced reads, which were then masked for low-complexity and low-quality sequence, and mapped to the mouse genome (mm9, whole genome). Cufflink was used to assemble transcripts and remap and quantify gene expression, which was estimated from FPKM (fragments per kilobase of exon model per million reads mapped) values. RNA-seq data were deposited in the GEO database repository with the accession number GSE125944.

**Skeletal visualization**

To visualize the distribution of bone and cartilage throughout mouse embryo skeletons at various stages of gestation, we stained embryo bones with Alizarin red S and Alcian blue. As much viscera and skin of the embryo as possible were removed while ensuring the integrity of the skeleton. Embryos were fixed overnight in 95% alcohol, and then stained overnight in Alcian blue staining solution and cleared with 95% alcohol. Embryos were then made transparent using 1% sodium hydroxide, subjected to Alizarin red staining, and cleared

with 1% KOH/20% glycerol. After staining, mouse embryonic skeletons were stored in 50% glycerol and photographed using an Axio Zoom V16 (Zeiss).

### Skeletal histological analysis

Consecutive paraffin mouse embryo sections were dewaxed in xylene, rehydrated with distilled water, then fixed in 4% paraformaldehyde/0.1 M phosphate buffer, and stained with Von Kossa and Safranin O-fast green staining kits (Servicebio). Stained sections were scanned using a panoramic MIDI scanner (3DHISTECH).

### Statistical analysis

Statistical analysis was carried out by GraphPad Prism version 8 ( $P < 0.05$  was considered significantly different). Statistical significance between the two groups was performed by unpaired two-tailed  $t$  tests, and between multiple groups was performed by one-way analysis of variance (ANOVA). All data are presented as mean  $\pm$  SEM; \* $P < 0.05$ , \*\* $P < 0.01$ , \*\*\* $P < 0.001$ , and \*\*\*\* $P < 0.0001$ . Original data are provided in data file S1.

### SUPPLEMENTARY MATERIALS

stm.sciencemag.org/cgi/content/full/12/537/eaax1798/DC1

Materials and methods

Fig. S1. Validation of rat anti-human/mouse PBX1 monoclonal antibody.

Fig. S2. The transcription factor PBX1 is more conserved than other related NK cell transcription factors.

Fig. S3. Expression of the GPFs, PTN and OGN, is up-regulated after overexpression of *PBX1* in dNK-like cells.

Fig. S4. *PBX1*<sup>G215</sup> retains DNA binding activity.

Fig. S5. dNK cells are the dominant subset expressing growth factors in early pregnancy.

Fig. S6. *PBX1* is highly expressed in uterine NK cells from pregnant *Pbx1*<sup>HA-tag</sup> knock-in mice.

Fig. S7. Knockout of *Pbx1* alters the gene expression profile in uterine NK cells, and the bone development of embryos is limited in pregnant *Pbx1*<sup>fl/fl</sup>; *Ncr1*<sup>Cre</sup> mice.

Fig. S8. Fetal growth is normal in pregnant *Eomes*<sup>NK-KO</sup> mice.

Fig. S9. Working model of *PBX1*<sup>+</sup> NK cells promoting early fetal development.

Table S1. Clinical data for patients with RSA and healthy controls.

Table S2. Commercial kits for cell preparation used in this study.

Table S3. Recombinant proteins used in this study.

Table S4. Antibodies used in this study.

Table S5. Human-specific primer sequences.

Table S6. Construction of siRNAs of the target gene.

Table S7. Primer sequences for the ChIP assay.

Table S8. Construction of oligonucleotides of *Pbx1*<sup>HA-tag</sup> knock-in mice.

Data file S1. Original data.

[View/request a protocol for this paper from Bio-protocol.](#)

### REFERENCES AND NOTES

- E. Vivier, D. Artis, M. Colonna, A. Diefenbach, J. P. Di Santo, G. Eberl, S. Koyasu, R. M. Locksley, A. N. J. McKenzie, R. E. Mebius, F. Powrie, H. Spits, Innate lymphoid cells: 10 years on. *Cell* **174**, 1054–1066 (2018).
- F.-D. Shi, H.-G. Ljunggren, A. La Cava, L. Van Kaer, Organ-specific features of natural killer cells. *Nat. Rev. Immunol.* **11**, 658–671 (2011).
- G. Eberl, J. P. Di Santo, E. Vivier, The brave new world of innate lymphoid cells. *Nat. Immunol.* **16**, 1–5 (2015).
- R. Vento-Tormo, M. Efremova, R. A. Botting, M. Y. Turco, M. Vento-Tormo, K. B. Meyer, J.-E. Park, E. Stephenson, K. Polaříski, A. Goncalves, L. Gardner, S. Holmqvist, J. Henriksson, A. Zou, A. M. Sharkey, B. Millar, B. Innes, L. Wood, A. Willbrey-Clark, R. M. Payne, M. A. Ivarsson, S. Liso, A. Filby, D. H. Rowitch, J. N. Bulmer, G. J. Wright, M. J. T. Stubbington, M. Haniffa, A. Moffett, S. A. Teichmann, Single-cell reconstruction of the early maternal–fetal interface in humans. *Nature* **563**, 347–353 (2018).
- H. Suryawanshi, P. Morozov, A. Straus, N. Sahasrabudhe, K. E. A. Max, A. Garzia, M. Kustagi, T. Tuschi, Z. Williams, A single-cell survey of the human first-trimester placenta and decidua. *Sci. Adv.* **4**, eaau4788 (2018).
- B. Fu, F. Wang, R. Sun, B. Ling, Z. Tian, H. Wei, CD11b and CD27 reflect distinct population and functional specialization in human natural killer cells. *Immunology* **133**, 350–359 (2011).
- P. C. Arck, K. Hecher, Fetomaternal immune cross-talk and its consequences for maternal and offspring's health. *Nat. Med.* **19**, 548–556 (2013).
- J. N. Bulmer, G. E. Lash, Uterine natural killer cells: Time for a re-appraisal? *F1000Res.* **8**, 1000 Faculty Rev-999 (2019).
- B. Fu, X. Li, R. Sun, X. Tong, B. Ling, Z. Tian, H. Wei, Natural killer cells promote immune tolerance by regulating inflammatory T<sub>H</sub>17 cells at the human maternal–fetal interface. *Proc. Natl. Acad. Sci. U.S.A.* **110**, E231–E240 (2013).
- S. Seshadri, S. K. Sunkara, Natural killer cells in female infertility and recurrent miscarriage: A systematic review and meta-analysis. *Hum. Reprod. Update* **20**, 429–438 (2014).
- B. Fu, Y. Zhou, X. Ni, X. Tong, X. Xu, Z. Dong, R. Sun, Z. Tian, H. Wei, Natural killer cells promote fetal development through the secretion of growth-promoting factors. *Immunity* **47**, 1100–1113.e6 (2017).
- S. M. Laird, E. M. Tuckerman, B. A. Cork, S. Linjawi, A. I. F. Blakemore, T. C. Li, A review of immune cells and molecules in women with recurrent miscarriage. *Hum. Reprod. Update* **9**, 163–174 (2003).
- D. W. Branch, M. Gibson, R. M. Silver, Clinical practice. Recurrent miscarriage. *N. Engl. J. Med.* **363**, 1740–1747 (2010).
- Y. B. Jeve, W. Davies, Evidence-based management of recurrent miscarriages. *J. Hum. Reprod. Sci.* **7**, 159–169 (2014).
- A. G. Freud, B. L. Mundy-Bosse, J. Yu, M. A. Caligiuri, The broad spectrum of human natural killer cell diversity. *Immunity* **47**, 820–833 (2017).
- A. A. Ashkar, J. P. Di Santo, B. A. Croy, Interferon- $\gamma$  contributes to initiation of uterine vascular modification, decidual integrity, and uterine natural killer cell maturation during normal murine pregnancy. *J. Exp. Med.* **192**, 259–270 (2000).
- J. Hanna, D. Goldman-Wohl, Y. Hamani, I. Avraham, C. Greenfield, S. Natanson-Yaron, D. Porgador, E. Keshet, T. I. Arnon, I. Manaster, R. Gazit, V. Yutkin, D. Benharroch, A. Porgador, E. Keshet, S. Yagel, O. Mandelboim, Decidual NK cells regulate key developmental processes at the human fetal-maternal interface. *Nat. Med.* **12**, 1065–1074 (2006).
- M. Gamliel, D. Goldman-Wohl, B. Isaacson, C. Gur, N. Stein, R. Yamin, M. Berger, M. Grunewald, E. Keshet, Y. Rais, C. Bornstein, E. David, A. Jelinski, I. Eisenberg, C. Greenfield, A. Ben-David, T. Imbar, R. Gilad, R. Haimov-Kochman, D. Mankuta, M. Elami-Suzin, I. Amit, J. H. Hanna, S. Yagel, O. Mandelboim, Trained memory of human uterine NK cells enhances their function in subsequent pregnancies. *Immunity* **48**, 951–962.e5 (2018).
- À. C. Crespo, J. L. Strominger, T. Tilburgs, Expression of KIR2DS1 by decidual natural killer cells increases their ability to control placental HCMV infection. *Proc. Natl. Acad. Sci. U.S.A.* **113**, 15072–15077 (2016).
- A. Moffett-King, Natural killer cells and pregnancy. *Nat. Rev. Immunol.* **2**, 656–663 (2002).
- P. Parham, A. Moffett, Variable NK cell receptors and their MHC class I ligands in immunity, reproduction and human evolution. *Nat. Rev. Immunol.* **13**, 133–144 (2013).
- L. J. Yockey, A. Iwasaki, Interferons and proinflammatory cytokines in pregnancy and fetal development. *Immunity* **49**, 397–412 (2018).
- J. P. Andreotti, A. E. Paiva, P. H. D. M. Prazeres, D. A. P. Guerra, W. N. Silva, R. S. Vaz, A. Mintz, A. Birbrair, The role of natural killer cells in the uterine microenvironment during pregnancy. *Cell. Mol. Immunol.* **15**, 941–943 (2018).
- F. Ficara, M. J. Murphy, M. Lin, M. L. Cleary, *Pbx1* regulates self-renewal of long-term hematopoietic stem cells by maintaining their quiescence. *Cell Stem Cell* **2**, 484–496 (2008).
- M. Sanyal, J. W. Tung, H. Karsunky, H. Zeng, L. Selleri, I. L. Weissman, L. A. Herzenberg, M. L. Cleary, B-cell development fails in the absence of the *Pbx1* proto-oncogene. *Blood* **109**, 4191–4199 (2007).
- Y. Xu, W. Zhao, S. D. Olson, K. S. Prabhakar, X. Zhou, Alternative splicing links histone modifications to stem cell fate decision. *Genome Biol.* **19**, 133 (2018).
- F. Colucci, J. Kieckbusch, Maternal uterine natural killer cells nurture fetal growth: *In medio stat virtus*. *Trends Mol. Med.* **21**, 60–67 (2015).
- E. Y. Chung, J. Liu, Y. Homma, Y. Zhang, A. Brendolan, M. Saggese, J. Han, R. Silverstein, L. Selleri, X. Ma, Interleukin-10 expression in macrophages during phagocytosis of apoptotic cells is mediated by homeodomain proteins *Pbx1* and *Prep-1*. *Immunity* **27**, 952–964 (2007).
- D. K. Sojka, B. Plougastel-Douglas, L. Yang, M. A. Pak-Wittel, M. N. Artyomov, Y. Ivanova, C. Zhong, J. M. Chase, P. B. Rothman, J. Yu, J. K. Riley, J. Zhu, Z. Tian, W. M. Yokoyama, Tissue-resident natural killer (NK) cells are cell lineages distinct from thymic and conventional splenic NK cells. *eLife* **3**, e01659 (2014).
- H. Peng, X. Jiang, Y. Chen, D. K. Sojka, H. Wei, X. Gao, R. Sun, W. M. Yokoyama, Z. Tian, Liver-resident NK cells confer adaptive immunity in skin-contact inflammation. *J. Clin. Invest.* **123**, 1444–1456 (2013).
- J.-M. Doisne, E. Balmes, S. Boulenouar, L. M. Gaynor, J. Kieckbusch, L. Gardner, D. A. Hawkes, C. F. Barbara, A. M. Sharkey, H. J. M. Brady, J. J. Brosens, A. Moffett, F. Colucci, Composition, development, and function of uterine innate lymphoid cells. *J. Immunol.* **195**, 3937–3945 (2015).

32. M. Ball, M. Carmody, F. Wynne, P. Dockery, A. Aigner, I. Cameron, J. Higgins, S. D. Smith, J. D. Aplin, T. Moore, Expression of pleiotrophin and its receptors in human placenta suggests roles in trophoblast life cycle and angiogenesis. *Placenta* **30**, 649–653 (2009).
33. T. Mikuni, J. Nishiyama, Y. Sun, N. Kamasawa, R. Yasuda, High-throughput, high-resolution mapping of protein localization in mammalian brain by in vivo genome editing. *Cell* **165**, 1803–1817 (2016).
34. M. A. Caligiuri, Human natural killer cells. *Blood* **112**, 461–469 (2008).
35. S. M. Gordon, J. Chaix, L. J. Rupp, J. Wu, S. Madera, J. C. Sun, T. Lindsten, S. L. Reiner, The transcription factors T-bet and Eomes control key checkpoints of natural killer cell maturation. *Immunity* **36**, 55–67 (2012).
36. E. Vivier, E. Tomasello, M. Baratin, T. Walzer, S. Ugolini, Functions of natural killer cells. *Nat. Immunol.* **9**, 503–510 (2008).
37. L. Selleri, M. J. Depew, Y. Jacobs, S. K. Chanda, K. Y. Tsang, K. S. E. Cheah, J. L. R. Rubenstein, S. O’Gorman, M. L. Cleary, Requirement for *Pbx1* in skeletal patterning and programming chondrocyte proliferation and differentiation. *Development* **128**, 3543–3557 (2001).
38. D. J. McCulley, M. D. Wienhold, E. A. Hines, T. A. Hacker, A. Rogers, R. J. Pewowaruk, R. Zewdu, N. C. Chesler, L. Selleri, X. Sun, PBX transcription factors drive pulmonary vascular adaptation to birth. *J. Clin. Invest.* **128**, 655–667 (2018).
39. C.-P. Chang, K. Stankunas, C. Shang, S.-C. Kao, K. Y. Twu, M. L. Cleary, *Pbx1* functions in distinct regulatory networks to pattern the great arteries and cardiac outflow tract. *Development* **135**, 3577–3586 (2008).
40. K. Karimi, M. E. Solano, A. A. Ashkar, H. Ho, E.-M. Steidle, K.-A. McVey Neufeld, K. Hecher, J. Bienenstock, P. C. Arck, Regulation of pregnancy maintenance and fetal survival in mice by CD27<sup>low</sup> mature NK cells. *J. Mol. Med.* **90**, 1047–1057 (2012).
41. D. Feyaerts, A. van der Meer, I. Joosten, R. G. van der Molen, Selective expansion and CMV-dependency in pregnancy trained human endometrial NK cells. *Cell. Mol. Immunol.* **16**, 410–411 (2019).
42. G. Murugappan, L. K. Shahine, C. O. Perfetto, L. R. Hickok, R. B. Lathi, Intent to treat analysis of in vitro fertilization and preimplantation genetic screening versus expectant management in patients with recurrent pregnancy loss. *Hum. Reprod.* **31**, 1668–1674 (2016).

**Funding:** This work was supported by the key project of the National Key R&D Program of China (no. 2018YFC1003900 to H.W.) and the National Natural Science Foundation of China

(nos. 81788101 to Z.T., 31900662 to Y. Zhou, and 31870914 to B.F.) and project funded by the China Postdoctoral Science Foundation (no. 2018M640596 to Y. Zhou) and the Anhui provincial Natural Science Foundation (no. 1908085QC101 to Y. Zhou). **Author contributions:** Y. Zhou designed and performed the experiments, analyzed and interpreted the data, and wrote the manuscript. B.F. designed, assisted with data interpretation, and wrote the manuscript. X.X. performed experiments on anti-PBX1 antibody purification and fluorescein labeling, identified mouse genotypes by PCR, and collected tissue samples. J.Z. was responsible for constructing *Pbx1*<sup>HA-tag</sup> knock-in mice. X.T., Y.W., Y. Zhai, and X.K. collected URSA samples and information from donors. Z.D., X.Z., and N.S. provided the genetic tool mice. R.S. assisted with data interpretation. Z.T. provided strategic planning, conceived the project, and interpreted some data. H.W. supervised the project, provided crucial ideas, assisted with data interpretation, and wrote the manuscript. **Competing interests:** H.W., Y. Zhou, X.X., J.Z., B.F., R.S., and Z.T. are inventors on patent application (CN201910037029.X.) submitted by the University of Science and Technology of China that covers the PBX1 antibody and its usage in recurrent spontaneous abortion. The other authors declare that they have no competing interests. **Data and materials availability:** All data and code to understand and assess the conclusions of this research are available in the main text, Supplementary Materials, and from the following repositories: ChIP-seq data files are available at <https://www.ncbi.nlm.nih.gov/geo/query/acc.cgi?acc=GSE110244> in the GEO database repository of the National Center for Biotechnology Information (NCBI) (accession number GSE110244), whole-exome sequencing data files are available at [www.ncbi.nlm.nih.gov/bioproject/517620](http://www.ncbi.nlm.nih.gov/bioproject/517620) in the NCBI SRA under BioProject PRJNA517620 (SRA: SRR8505897-8505904), and RNA-seq of mouse uterine NK cells data files are available at [www.ncbi.nlm.nih.gov/geo/GSE125944](http://www.ncbi.nlm.nih.gov/geo/GSE125944) in the GEO database repository (accession number GSE125944). Resources and reagents are available from Z.T. and H.W. under a material transfer agreement with the University of Science and Technology of China.

Submitted 28 February 2019  
Resubmitted 19 November 2019  
Accepted 12 February 2020  
Published 1 April 2020  
10.1126/scitranslmed.aax1798

**Citation:** Y. Zhou, B. Fu, X. Xu, J. Zhang, X. Tong, Y. Wang, Z. Dong, X. Zhang, N. Shen, Y. Zhai, X. Kong, R. Sun, Z. Tian, H. Wei, PBX1 expression in uterine natural killer cells drives fetal growth. *Sci. Transl. Med.* **12**, eaax1798 (2020).

## PBX1 expression in uterine natural killer cells drives fetal growth

Yonggang Zhou, Binqing Fu, Xiuxiu Xu, Jinghe Zhang, Xianhong Tong, Yanshi Wang, Zhongjun Dong, Xiaoren Zhang, Nan Shen, Yiwen Zhai, Xiangdong Kong, Rui Sun, Zhigang Tian and Haiming Wei

*Sci Transl Med* 12, eaax1798.  
DOI: 10.1126/scitranslmed.aax1798

### Natural killers' gentler side

Numerous decidual natural killer cells are found at the maternal-fetal interface in the placenta during early pregnancy. Zhou *et al.* identified a transcription factor called PBX1, which is present in these natural killer cells and stimulates the production of growth-promoting factors, proteins needed for fetal growth and development. In pregnant mice, lack of functional PBX1 in decidual natural killer cells resulted in fetal growth restriction, which could be rescued by reintroducing wild-type PBX1. Human patients with a history of unexplained recurrent spontaneous abortion often had impaired activity of PBX1 in their decidual natural killer cells as well, offering a mechanistic explanation for their diagnosis.

#### ARTICLE TOOLS

<http://stm.sciencemag.org/content/12/537/eaax1798>

#### SUPPLEMENTARY MATERIALS

<http://stm.sciencemag.org/content/suppl/2020/03/30/12.537.eaax1798.DC1>

#### RELATED CONTENT

<http://stm.sciencemag.org/content/scitransmed/11/474/eaaf7533.full>  
<http://stm.sciencemag.org/content/scitransmed/10/438/eaan2263.full>  
<http://stm.sciencemag.org/content/scitransmed/7/276/276ra25.full>  
<http://stm.sciencemag.org/content/scitransmed/6/238/238ra72.full>

#### REFERENCES

This article cites 42 articles, 9 of which you can access for free  
<http://stm.sciencemag.org/content/12/537/eaax1798#BIBL>

#### PERMISSIONS

<http://www.sciencemag.org/help/reprints-and-permissions>

Use of this article is subject to the [Terms of Service](#)

---

*Science Translational Medicine* (ISSN 1946-6242) is published by the American Association for the Advancement of Science, 1200 New York Avenue NW, Washington, DC 20005. The title *Science Translational Medicine* is a registered trademark of AAAS.

Copyright © 2020 The Authors, some rights reserved; exclusive licensee American Association for the Advancement of Science. No claim to original U.S. Government Works